Fig. 2

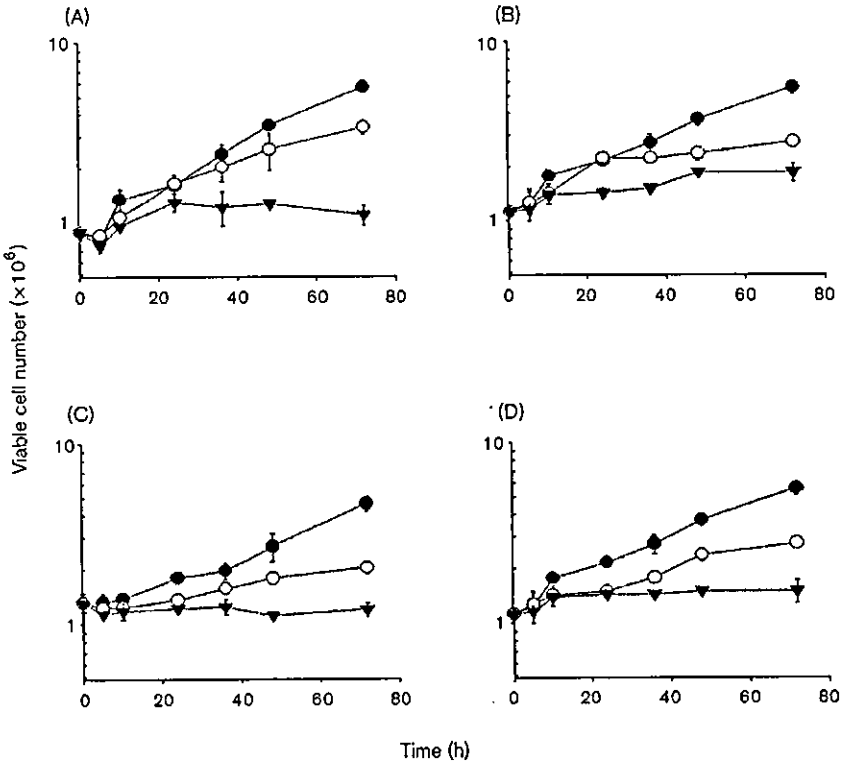

Growth curves of SNU-1 cells when incubated with (open circles, solid triangles) and without (solid circles) drug treatment: LOHP (A), 5-FU (B), PTX (C) and gefitinib (D). Cells were treated at two different concentrations near the IC_{50} (open circles) and the IC_{80} (solid triangles). The concentrations were: 0.75 and 7.55 μM for LOHP, 9 and 65 μM for 5-FU, 2.5 and 10 nM for PTX, and 13 and 38 μM for gefitinib. For cell number counting, cells were harvested by resuspending in medium and counted using a Coulter counter. Trypan blue exclusion was used for the determination of viable cell fraction.

cycle arrest effects contributes significantly to the overall growth inhibition induced by LOHP and PTX.

Cell cycle arrest effect with single drug treatment

The cell cycle arrest effect of the four agents was studied following a single drug exposure at two different concentrations for 72 h, i.e. around IC_{50} and IC_{80} as determined from the MTT dose–response curves. For LOHP, exposure to IC_{50} level concentrations, 0.75 μM did not induce significant changes in the cell cycle distribution (Fig. 3). When exposed to IC_{80} level concentrations, 7.55 μM of LOHP showed a moderate S phase decrease and G_2/M phase increase. Exposure to 5-FU (9 and 65 μM) resulted in an S phase increase along with G_2/M phase decreases in a concentration dependent manner: the cell cycle change following 5-FU treatment at the higher concentration (IC_{80}) was more pronounced. For LOHP and 5-FU, the sub-G_1 population, representative of cells that had undergone apoptosis, increased with time- and concentration-dependent manner. For PTX, cell cycle effect was dependent on drug concentration. At IC_{50} (2.5 nM), the number of cells in G_1 phase decreased with rapid accumulation of cells in sub-G_1 phase. At 10 nM, however, most cells were blocked in G_2/M phase (69.5 ± 0.8%) and a parallel decrease of the G_1 population was observed at 24 h, and a significant increase of the sub-G_1 population (27.4 ± 0.4%) and polyploid cells with ≥ 4*n* at 72 h. Gefitinib (13 and 38 μM) also showed a concentration dependent pattern of G_1 phase cell cycle arrest. The sub-G_1 population was induced after 72 h exposure at IC_{50} concentration (12.5 ± 1.6%) and increased to 52% after 72 h exposure at the concentration of 38 μM.

Evaluation of synergism

We evaluated the synergistic interaction between the cytotoxic agents, LOHP, 5-FU or PTX, and the cytostatic agent, gefitinib. All combinations were given at equitoxic ratios at the 50% inhibition levels of each drug, i.e. IC_{50} of drug A:IC_{50} of drug B. The dose–response curves are shown in Fig. 4 and the CI_x values calculated for $0.2 \leq f_a \leq 0.8$ (i.e. $20 \leq x \leq 80$) are shown in Fig. 5. CI_x values for the combination LOHP + gefitinib varied with f_a: CI_x decreased from 1.74 at $f_a = 0.2$ to 0.67 at $f_a = 0.8$. In the clinically relevant range of $f_a \geq 0.5$, hence, LOHP + gefitinib was considered to be synergistic to

Fig. 6

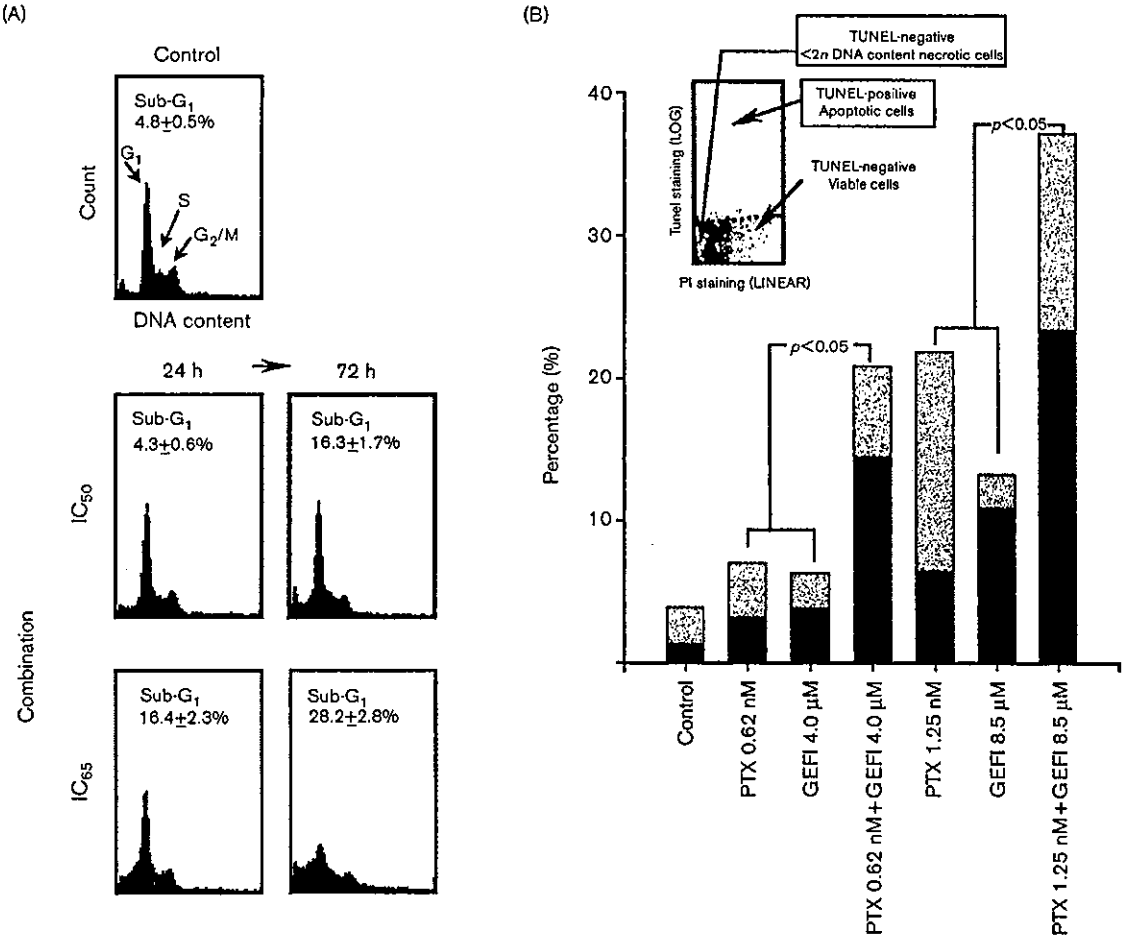

Cell cycle distribution and apoptosis induction during simultaneous treatment with PTX and gefitinib in SNU-1 cells. The drug concentrations used were 0.6 nM PTX + 4 μM (IC_{50}) or 1.25 nM PTX + 8.5 μM gefitinib (IC_{65}). (A) Representative histograms are shown for 24 and 72 h post-treatment with the percentage of cells in the sub-G_1 phase. At predetermined times following drug exposure, cells were harvested, fixed, stained with propidium iodide (PI) and analyzed by flow cytometry. (B) The bivariate analysis of DNA content and apoptosis in cells exposed to the indicated drug treatment for 72 h. Cells were treated for 72 h and processed for the double staining of TUNEL/PI and analyzed by flow cytometry. Solid box: TUNEL-negative necrotic cells; gray box: TUNEL-positive apoptotic cells. Statistical analysis: sum of PTX and gefitinib alone versus combination: $p<0.05$.

demonstrated in a wide range of human cancer cell lines, and the reported IC_{50}s of gefitinib vary by cell line and by the assay method used. A soft agar colony assay showed an IC_{50} range of 0.05–2.5 μM for gefitinib in breast, colon and gastric cancer cells [8,21]. On the other hand, an IC_{50} range of 6–30 μM was reported in human head/neck and colon cancer cells by MTT [22,23]. Our results on the antitumor activity of gefitinib in SNU-1 cells are comparable with those obtained using the same viability assay method, i.e. MTT (Table 1).

A few studies have demonstrated an inverse correlation between growth IC_{50} and EGFR expression level [22], whereas contradictory data have been reported by others [7]. SNU-1 cells express moderate levels of EGFR, which may explain its moderate IC_{50} compared to other studies, which used highly overexpressing cell lines, such as A431. The EGFR signaling pathway involves the activation of several nuclear proteins, including cyclin D_1, via the activation of *ras* and mitogen-activated protein kinase [21]. Since EGFR activates cyclin D_1, and cyclin D_1 is required for cell cycle progression from G_1 to the S phase, EGFR signaling is critical for cell proliferation and its inhibition causes G_1 arrest in human cancer cells [21]. Our results also demonstrate that the inhibition of EGFR signaling by gefitinib induces G_1 arrest in human gastric cancer cells in a concentration dependent manner (Fig. 3).

In common with other cytostatic agents, gefitinib is expected to be a good candidate for combination regimens with cytotoxic agents. The combination of gefitinib + PTX has been shown to induce dose-depen-

dent cooperative growth inhibition and the potentiation of apoptosis *in vitro* [8,21], and to induce complete regression in some human tumor xenograft models [7]. Gefitinib + LOHP has been found to be supra-additive in human ovarian, breast and colon cells [14,24]. The sequence-dependent synergy appeared to be cell-line specific, i.e. gefitinib followed by cisplatin/5-FU was synergistic in head/neck cell cancer cell line [22], whereas gefitinib followed by oxaliplatin was antagonistic in human colon cancer cell line [25]. The simultaneous exposure was additive to synergistic in both studies, hence, the simultaneous schedule was to chosen to evaluate the synergy in the present study. We did not evaluate the sequence-dependent interactions because SNU-1 cells grow as a suspension and, hence, are not suitable for such experiments. The sequence dependency should be investigated using another human gastric cancer cell line.

In the present study, CI_x was calculated for the range of $0.2 \leq f_a \leq 0.8$ (Fig. 5), but the combination effect on cell cycle distribution and apoptosis induction was evaluated for the range of $f_a \geq 0.5$, i.e. at IC_{50} and IC_{80} levels (Fig. 6). Considering the fact that the maximum effect is needed in the clinical situation, it should be more relevant to focus on the effect above IC_{50} level [22]. Preclinical studies (especially, animal models) commonly use lower doses of chemotherapy to observe greater synergy; however, this often do not translate to the clinic, where maximum therapeutic doses are used [26].

In our study, the potentiation of antitumor activity was greatest for PTX + gefitinib, which had the lowest CI_{50} value among the three combinations and moreover the resistant fraction in the PTX single treatment was completely abrogated (Figs 4 and 5). LOHP + gefitinib is also a promising combination regimen because it produced a very similar level of synergism to PTX + gefitinib at $f_a = 0.8$ and additive effects at the $f_a = 0.5$ level. Gefitinib combined with PTX resulted in enhanced drug-induced apoptosis (Fig. 6). It is conceivable that the cytotoxicity of PTX is potentiated by the effective inhibition of survival signals upregulated by the EGFR signal network. The elucidation of the mechanism of this interaction requires further investigation.

Results of phase III lung trials for gefitinib + cytotoxics were disappointing and can be attributed to many factors including the following: (i) due to the lack of correlation between the apparent expression of EGFR and sensitivity, the responding phenotype was not known and patient selection could not be made, (ii) it is believed that triplet regimen of conventional chemotherapy are not superior to doublets in non-small cell lung cancer, and (iii) patients (in IDEAL phase II trials) who were already heavily treated with, and refractory to, chemotherapy may have been more sensitive to the inhibition of the EGFR pathway by gefitinib [27]. Despite the negative results of phase III lung trials, the rationales for studying the combination of gefitinib with cytotoxics in gastric cancers are 3-fold. (i) EGFR levels were associated with poor prognosis in gastric cancer patients [28,29], (ii) gefitinib is given orally, hence, higher drug concentration can be obtained in the gastric tissues and (iii) gastric cancers are relatively easy for biopsy study through which the responding phenotype can be identified.

In summary, the present study demonstrates that the antitumor activity of gefitinib, against human gastric carcinoma cells, is accompanied by significant cell cycle arrest and apoptosis. We also found that the antiproliferative effects of the cytotoxic drugs, LOHP and PTX, could be greatly enhanced when combined with gefitinib. The suppression of growth by gefitinib may be of clinical importance as the prolonged administration of orally active gefitinib could offer long-term control of gastric tumor growth and metastasis. This study provides preclinical data supporting the clinical development of gefitinib and its use in combination with PTX or LOHP against MMR-deficient human gastric cancers that express EGFR. Moreover, this study shows that gefitinib warrants further evaluation *vis-à-vis* its use in other gastric cancer cells/tumors.

References

1 Kim YH, Shin SW, Kim BS, Kim JH, Kim JG, Mok YJ, *et al.* Paclitaxel, 5-FU, and cisplatin combination chemotherapy for the treatment of advanced gastric carcinoma. *Cancer* 1999; 85:295–301.

2 Slesak B, Harlozinska A, Porebska I, Bojarowski T, Lapinska J, Rzeszutko M, *et al.* Expression of epidermal growth factor receptor family proteins (EGFR, c-erbB-2 and c-erbB-3) in gastric cancer and chronic gastritis. *Anticancer Res* 1998; 18:2727–2732.

3 Aoyagi K, Kohfuji K, Yano S, Murakami N, Miyagi M, Takeda J, *et al.* Evaluation of the epidermal growth factor receptor (EGFR) and c-erbB-2 in superspreading-type and penetrating-type gastric carcinoma. *Kurume Med J* 2001; 48:197–200.

4 Piontek M, Hengels KJ, Porschen R, Strohmeyer G. Antiproliferative effect of tyrosine kinase inhibitors in epidermal growth factor-stimulated growth of human gastric cancer cells. *Anticancer Res* 1993; 13:2119–2123.

5 Mendelsohn J, Fan Z. Epidermal growth factor receptor family and chemosensitization. *J Natl Cancer Inst* 1997; 89:341–343.

6 Caputo R, Tuccillo C, Manzo BA, Zarrilli R, Tortora G, Blanco Cdel V, *et al.* *Helicobacter pylori* VacA toxin up-regulates vascular endothelial growth factor expression in MKN 28 gastric cells through an epidermal growth factor receptor-, cyclooxygenase-2-dependent mechanism. *Clin Cancer Res* 2003; 9:2015–2021.

7 Sirotnak FM, Zakowski MF, Miller VA, Scher HI, Kris MG. Efficacy of cytotoxic agents against human tumor xenografts is markedly enhanced by coadministration of ZD1839 (Iressa), an inhibitor of EGFR tyrosine kinase. *Clin Cancer Res* 2000; 6:4885–4892.

8 Ciardiello F, Caputo R, Borriello G, Del Bufalo D, Biroccio A, Zupi G, *et al.* ZD1839 (IRESSA), an EGFR-selective tyrosine kinase inhibitor, enhances taxane activity in *bcl*-2 overexpressing, multidrug-resistant MCF-7 ADR human breast cancer cells. *Int J Cancer* 2002; 98:463–469.

9 Bevilacqua RA, Simpson AJ. Methylation of the hMLH1 promoter but no hMLH1 mutations in sporadic gastric carcinomas with high-level microsatellite instability. *Int J Cancer* 2000; 87: 200–203.

10 Kang YH, Bae SI, Kim WH. Comprehensive analysis of promoter methylation and altered expression of hMLH1 in gastric cancer cell lines with microsatellite instability. *J Cancer Res Clin Oncol* 2002; 128:119–124.

11 Fink D, Aebi S, Howell SB. The role of DNA mismatch repair in drug resistance. *Clin Cancer Res* 1998; 4:1–6.

12 Shin KH, Yang YM, Park J-G. Absence or decreased levels of the hMLH-1 protein in human carcinoma cell lines: implication of hMLH-1 in alkylation tolerance. *J Cancer Res Clin Oncol* 1998; **124**:421–426.

13 Raymond E, Faivre S, Woynarowski JM, Chaney SG. Oxaliplatin: mechanism of action and antineoplastic activity. *Semin Oncol* 1998; **25**:4–12.

14 Ciardiello F, Caputo R, Bianco R, Damiano V, Pomatico G, De Placido S, *et al.* Antitumor effect and potentiation of cytotoxic drugs activity in human cancer cells by ZD-1839 (Iressa), an epidermal growth factor receptor-selective tyrosine kinase inhibitor. *Clin Cancer Res* 2000; **6**:2053–2063.

15 Carethers JM, Chauhan DP, Fink D, Nebel S, Bresalier RS, Howell SB, *et al.* Mismatch repair proficiency and *in vitro* response to 5-fluorouracil. *Gastroenterology* 1999; **117**:123–131.

16 Carmichael J, Mitchell JB, DeGraff WG, Gamson J, Gazdar AF, Johnson BE, *et al.* Chemosensitivity testing of human lung cancer cell lines using the MTT assay. *Br J Cancer* 1988; **57**:540–547.

17 Chou TC, Talalay P. Quantitative analysis of dose–effect relationships: the combined effects of multiple drugs or enzyme inhibitors. *Adv Enz Reg* 1984; **22**:27–55.

18 Kuh HJ, Nakagawa S, Usuda J, Yamaoka K, Saijo N, Nishio K. A computational model for quantitative analysis of cell cycle arrest and its contribution to overall growth inhibition by anticancer agents. *Jpn J Cancer Res* 2000; **91**:1303–1313.

19 Steel GG. *Growth Kinetics of Tumors: Cell Population Kinetics in Relation to the Growth and Treatment of Cancer.* Oxford: Clarendon Press; 1977.

20 Honecker F, Kollmannsberger C, Quietzsch D, Haag C, Schroeder M, Spott C, *et al.* Phase II study of weekly paclitaxel plus 24-h continuous infusion 5-FU, folinic acid and 3-weekly cisplatin for the treatment of patients with advanced gastric cancer. *Anticancer Drugs* 2002; **13**:497–503.

21 Ciardiello F, Caputo R, Bianco R, Damiano V, Fontanini G, Cuccato S, *et al.* Inhibition of growth factor production and angiogenesis in human cancer cells by ZD1839 (Iressa), a selective epidermal growth factor receptor tyrosine kinase inhibitor. *Clin Cancer Res* 2001; **7**: 1459–1465.

22 Magne N, Fischel JL, Dubreuil A, Formento P, Marcie S, Lagrange JL, *et al.* Sequence-dependent effects of ZD1839 ('Iressa') in combination with cytotoxic treatment in human head and neck cancer. *Br J Cancer* 2002; **86**:819–827.

23 Magne N, Fischel JL, Dubreuil A, Formento P, Poupon MF, Laurent-Puig P, *et al.* Influence of epidermal growth factor receptor (EGFR), p53 and intrinsic MAP kinase pathway status of tumour cells on the antiproliferative effect of ZD1839 ('Iressa'). *Br J Cancer* 2002; **86**:1518–1523.

24 Xu JM, Azzariti A, Colucci G, Paradiso A. The effect of gefitinib (Iressa, ZD1839) in combination with oxaliplatin is schedule-dependent in colon cancer cell lines. *Cancer Chemother Pharmacol* 2003; **52**:442–448.

25 Xu JM, Azzariti A, Severino M, Lu B, Colucci G, Paradiso A. Characterization of sequence-dependent synergy between ZD1839 ('Iressa') and oxaliplatin. *Biochem Pharmacol* 2003; **66**:551–563.

26 Herbst RS, Giaccone G, Schiller JH, Natale RB, Miller V, Manegold C, *et al.* Gefitinib in combination with paclitaxel and carboplatin in advanced non-small-cell lung cancer: a phase III trial—INTACT 2. *J Clin Oncol* 2004; **22**:785–794.

27 Gamboa-Dominguez A, Dominguez-Fonseca C, Quintanilla-Martinez L, Reyes-Gutierrez E, Green D, Angeles-Angeles A, *et al.* Epidermal growth factor receptor expression correlates with poor survival in gastric adenocarcinoma from Mexican patients: a multivariate analysis using a standardized immunohistochemical detection system. *Mod Pathol* 2004; **17**:579–587.

28 Kopp R, Rothbauer E, Ruge M, Arnholdt H, Spranger J, Muders M, *et al.* Clinical implications of the EGF receptor/ligand system for tumor progression and survival in gastrointestinal carcinomas: evidence for new therapeutic options. *Recent Results Cancer Res* 2003; **162**:115–132.

29 Perez-Soler R. HER1/EGFR targeting: refining the strategy. *Oncologist* 2004; **9**:58–67.

Translational research for lung cancer – An update

K. Nishio[1], S. Korfee[1,2], W. Eberhardt[2], N. Saijo[1], and T. Tamura[1]

[1]*Shien-Lab, Medical Oncology, National Cancer Center Hospital and Pharmacology Division, National Cancer Center Research Institute, Tokyo, Japan.*
[2]*Department of Internal Medicine, West German Cancer Centre, Essen, Germany*

Correlative studies at the National Cancer Center Hospital

Molecular correlative studies are essential for the development of anticancer molecular target drugs. One of the major purposes of a correlative study is "proof of principle" (POP). However, clinical POP studies for small molecules are usually more difficult to complete than POP studies for antibodies[1].

Since 2001, the National Cancer Center Hospital (Tokyo, Japan) has been operating as a laboratory for translational studies to develop molecular correlative studies. The laboratory members consist of medical oncologists, basic researchers, CRC research fellows, invited researchers from abroad, technicians, and statisticians. The laboratory is located next to the phase I wards in the hospital, enabling more than ten molecular correlative studies to be simultaneously performed. New clinical samples can be quickly obtained from patients (including outpatients), prepared for storage, and stored in the laboratory. The medical doctors working in the laboratory are often research fellows supported by government grants, since these individuals are often interested in this kind of research.

The location of the laboratory also gives medical oncologists the opportunity to frequently communicate with research members. The significance of study endpoints, study designs, technical and statistical information, and feasibility are frequently discussed, especially among young medical oncologists and researchers. As a result, young oncologists and researchers often collaborate in the proposal of new molecular correlative studies.

The major activities of the laboratory are pharmacokinetics or pharmacodynamics studies for early clinical studies (PI and PII) and reverse translational studies. Tissue banking and quality control are two of the most important activities. Part of the clinical sample testing is performed in collaboration with the CRO.

Gene expression profiles

Gene expression arrays (DNA chips) have already been used in clinical studies to predict response and in POP studies. Many kinds of DNA chips are now available. Oligonucleotide arrays containing more than 40,000 genes have recently become popular. These chips can be used differentially, depending upon the study's purpose. Before clinical use, however, an array's quality (linearity and reproducibility) should be determined in preclinical studies. At our center, the quality of each array is evaluated and expressed as the Pearson's product-moment coefficient of correlation. Based on the validated quality of the cDNA, protocols based on "experienced designs" are then established.

In clinical settings, sample quality and feasibility are often major limitations in the design of new studies. To maintain the quality of clinical samples, a system for sample flow has been established. First the purity of the nucleotides must be carefully examined. Purification methods largely depend on the tumor types. For example, brain tumors contain large amounts of carbohydrate chains, lung cancer samples are sometimes very hard, and breast cancer biopsy samples are lipid rich. These sample characteristics influence purification quality and efficiency.

After the gene expression profiles have been obtained for each samples, the data is analyzed using standardization, clustering, statistical analysis, and validation methods. Statistical and biological validation is essential. Ideally, clinical cross-validation studies should be performed for independent clinical studies. On the other hand, biomarkers can be validated in the same clinical study using the "leave-one out" method. The endpoint of these correlative studies is usually the selection of biomarkers for predicting response or toxicity. For such endpoints, the quality of the clinical study itself is also very important.

We have also used another endpoint in early clinical studies. We compared the clinical samples obtained before and after treatment. Analysis of gene alterations after treatment can be utilized for POP. We completed these correlative studies as part of clinical studies for multitarget tyrosine kinase inhibitors, farnesyl transferase inhibitor, and cytotoxic drugs.

For biological confirmation, we usually perform (semi-)quantitative RT-PCR or immunostaining. However, we recently discovered that "pathway analysis" is a powerful method for improving our understanding of the alteration of genes related to biological signal transduction

pathways. For the analysis of transcription factors, "network analysis" can be used to identify the signaling pathways of the transcription factors.

Correlative Study for TKI using New Array

We have several developed new arrays in collaboration with biocompanies as follows;.

Fiber Array To differentially identify the isotypes of target genes, such as beta-tubulin, we have developed a customized, highly quantitative "fiber array" for "antimitotic inhibitors". We will analyze the isotype-specific expression profile of beta-tubulin using this array.

Genotyping Array Recently, the EGFR mutation has become an exciting topic in research on tyrosine kinase inhibitors (TKI). Mutation analysis is now essential for any correlative studies for TKI. Patients with tumors containing the EGFR mutation in different exons are thought to have different responses to TKI[2, 3]. Whole exon (and intron) analysis can now be performed using the chip technology available in our laboratory. Additional mutations after treatment are also generating interest with regard to their role in acquired resistance to TKI.

Arrays for proteins Proteomics technology has been developed and successfully used to identify biomarkers for target-based drugs in a few clinical studies. Additional approaches, such as antibody arrays and "power blots", especially those using phospho-specific antibodies, should enable us to perform "kinome" analyses. Thus, these protein analysis technologies are now powerful tools for research on tyrosine kinase inhibitors.

References

1. Saijo N, Nishio K, Tamura T. Translational and clinical studies of target-based cancer therapy. *Int J Clin Oncol* 2003;8:187-92.0
2. Lynch TJ, Bell DW, Sordella R, Gurubhagavatula S, Okimoto RA, Brannigan BW, Harris PL, Haserlat SM, Supko JG, Haluska FG, Louis DN, Christiani DC, Settleman J, Haber DA. Activating mutations in the epidermal growth factor receptor underlying responsiveness of non-small-cell lung cancer to gefitinib. *N Engl J Med* 2004;350:2129-39.0
3. Paez JG, Janne PA, Lee JC, Tracy S, Greulich H, Gabriel S, Herman P, Kaye FJ, Lindeman N, Boggon TJ, Naoki K, Sasaki H, Fujii Y, Eck MJ, Sellers WR, Johnson BE, Meyerson M. EGFR mutations in lung cancer: correlation with clinical response to gefitinib therapy. *Science* 2004;304:1497-500.0

Int. J. Cancer: 108, 679–685 (2004)

Publication of the International Union Against Cancer

hnRNP L ENHANCES SENSITIVITY OF THE CELLS TO KW-2189

Fumiko TAGUCHI[1,3], Hitoshi KUSABA[1], Akira ASAI[4], Yasuo IWAMOTO[1], Keiichi YANO[4], Hirofumi NAKANO[4], Tamio MIZUKAMI[4], Nagahiro SAIJO[2], Harubumi KATO[3] and Kazuto NISHIO[1]*

[1]*Pharmacology Division, National Cancer Center Research Institute, Tokyo, Japan*
[2]*Medical Oncology Division, National Cancer Center Hospital, Tokyo, Japan*
[3]*Department of Surgery, Tokyo Medical University, Tokyo, Japan*
[4]*Tokyo Research Laboratories, Kyowa Hakko Kogyo Co. Ltd, Tokyo, Japan*

Heterogeneous nuclear ribonucleoproteins (hnRNPs) are involved in several RNA-related biological processes. We demonstrated hnRNP L as a candidate protein of DARP (duocarmycin-DNA adduct recognizing protein) by gel shift assay and amino acid sequencing. Stable transfectants of hnRNP L showed high sensitivity of the cells to the growth inhibitory effect of KW-2189, a duocarmycin derivative *in vitro*. Immunostaining of hnRNP L demonstrated differential intracellular localization of hnRNP L among human lung cancer cell lines. A transfection study using a series of deletion mutants of hnRNP L fused to indicated that the N-terminal portions of RRM(RNA recognition motif)1, RRM3 and RRM2 are involved in localization of hnRNP L. We identified sequences in these portions that have high homology with the sequences of known NLS (nuclear localization signal) and NES (nuclear export signal). hnRNP L is a factor that determines the sensitivities of cancer cells to the minor groove binder, and overexpression and differential intracellular localization of hnRNP L are involved in its function in lung cancer.

Key words: *hnRNP L; KW-2189; duocarmycin; minor groove binder; nuclear localization signal*

Heterogeneous nuclear ribonucleoproteins (hnRNPs) participate in a variety of processes involving RNA, including transcription, splicing, processing, translation and turnover, and there are approximately 20 major members of the hnRNP family.[1] High expression of some of these have been reported in several human malignant tumors and interest in the action of these proteins in malignancies has been growing.[2,3] HnRNP L is 68 kDa protein with 4 RNA recognition motifs (RRM). There have been several interesting reports demonstrating that cytoplasmic hnRNP L specifically interacts with VEGF mRNA in hypoxic cells *in vivo*, regulates VEGF mRNA stability[4] and binds in a sequence-specific manner to a *cis*-acting RNA sequence element that enables intron-independent gene expression.[5] The role of hnRNP L, however, still requires further study.

KW-2189 is a water-soluble derivative of antitumor antibiotic duocarmycin (DUM),[6–8] and DUM and its derivatives have been reported to exert their anti-tumor activity through covalent binding to the DNA minor groove and inhibition of DNA synthesis. We identified previously a nuclear protein DARP (duocarmycin-DNA adduct recognizing protein) in human cervical carcinoma HeLa S3 cells.[9] We purified the DARP from nuclear extract of HeLa S3 and its amino acid sequence was identical to hnRNP L. We investigated this, particularly in cancer cells.

MATERIAL AND METHODS

Cell cultures and reagents

Human small cell lung cancer cell lines SBC-3 and H69, human non-small cell lung cancer cell lines PC-14, and their respective cisplatin-resistant cell lines (SBC-3/CDDP, H69/CDDP,[10] and PC-14/CDDP[11]) were maintained in RPMI 1640 (Sigma, St. Louis, MO) supplemented with 10% heat-inactivated FBS (Gibco BRL, Gaithersburg, MD). Murine fibroblast cell line NIH3T3 and sublines (including cDNA transfectants) were cultured in DMEM (Nissui Pharmaceutical Co. Ltd., Tokyo, Japan) supplemented with 10% FBS. KW2189 was provided by Kyowa Hakko Kogyo Co., Ltd. A monoclonal antibody specific for hnRNP L (4D11) was generously provided by Dr. G. Dreyfuss (University of Pennsylvania, Philadelphia).

Cell extracts

Cells were washed twice with cold PBS and lysed in buffer (10 mM Tris-HCl pH 7.8, 1% Nonidet P-40, 0.15 M NaCl, 1 mM EDTA, 10 μg/ml aprotinin, 0.5 μg/ml leupeptin, 1 mM phenylmethane-sulfonyl fluoride [PMSF], 1 tablet/50 ml ϕgrComplete™ and 10% glycerol) for 60 min on ice. The lysates were centrifuged at 8,000*g* for 20 min, and supernatants were obtained as total protein. Protein concentration was measured by bicinchoninic acid protein assay (Pierce, Rockford, IL).

SBC-3, PC-14 and H69 cells were lysed in buffer A containing 10 mM HEPES-KOH (pH 7.9), 10 mM KCl, 0.1 mM EDTA-NaOH (pH 8.0), 0.1 mM ethyleneglycol bis(2-aminoethyl ether) tetraacetic acid (EGTA), 1 mM dithiothreitol (DTT), 0.5 mM PMSF, 1 mM aprotinin, and leupeptin. Nonidet P-40 (final concentration 0.5%) was added after allowing to stand on ice for 15 min. The supernatant obtained by centrifugation at 7,000*g* for 30 sec after standing on ice for 5 min was collected as the cytoplasmic fraction. The pellet was resuspended with buffer A containing 0.25 M sucrose, and after buffer B′ (buffer A containing 0.6 M sucrose) was added, the solution was centrifuged at 5,000*g* for 1 min at 4°C. The nuclei, which were contained in the pellet, were sonicated in buffer C containing 20 mM HEPES-KOH (pH 7.9), 0.4 M NaCl, 1 mM EDTA-NaOH (pH 8.0), 1 mM EGTA, 1 mM DTT and 1 mM PMSF, and then rocked at 4°C for 30 min and centrifuged at 8,000*g* for 10 min. The supernatant was used as the nuclear fraction. The nuclear protein content was adjusted to 5 μg per well, and the same volume of cytoplasmic protein was applied to the next well. The cytoplasmic and nuclear fractions were subjected to SDS-PAGE and Western blotting with anti-hnRNP L antibody.

Western blotting

An INSTA-Blot human tissues membrane (Imgenex, San Diego, CA), which contains 10 μg per lane of different human tissue lysates, was soaked in 100% methanol and then washed with TBST. After blocking the membrane in 5% skim milk in TBST for 1 hr at room temperature, it was probed with anti-hnRNP L antibody diluted (1:500) in TBST with 1% skim milk for 1 hr at

Fumiko Taguchi is a recipient of Research Resident Fellowship from the Foundation for Promotion of Cancer Research in Japan

*Correspondence to: Pharmacology Division, National Cancer Center Research Institute, 5-1-1 Tsukiji, Chuo-ku, Tokyo 104-0045, Japan. Fax: +81-3-3547-5185. E-mail: knishio@gan2.res.ncc.go.jp

Received 16 September 2002; Revised 25 August 2003; Accepted 12 September 2003

DOI 10.1002/ijc.11616

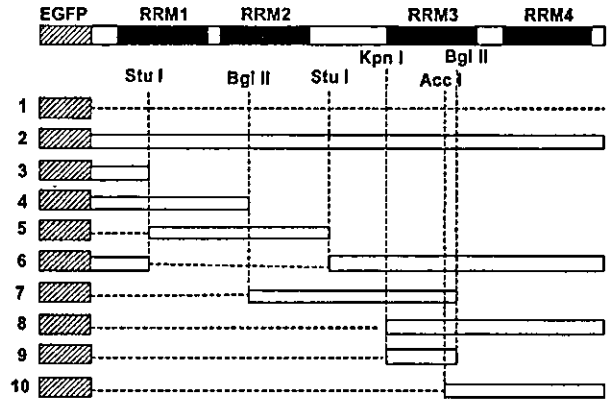

FIGURE 1 – Diagram of EGFP-hnRNP L deletion mutants. Known motifs, RNA recognition motifs (RRMs) 1, 2, 3 and 4 are boxed. The dark gray box denotes EGFP. Ten plasmids containing various parts of hnRNP L were constructed. The restriction sites used to generate deletion mutants are indicated.

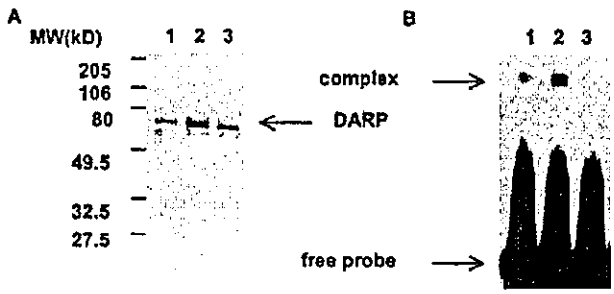

FIGURE 2 – Purification of DARP. (*a*) SDS-PAGE analysis of DEAE-sephacel fractions. *Lane 1*, 0.15 M KCl eluate; *Lane 2*, 0.2 M KCl eluate; *Lane 3*, 0.25 M KCl eluate. (*b*) Gel mobility shift assay of DEAE-sephacel fractions. *Lane 1*, 0.15 M KCl eluate; *Lane 2*, 0.2 M KCl eluate; *Lane 3*, 0.25 M KCl eluate. The oligonucleotides used as a probe contains the 5'-ATTA-3' sequence recognized by DUMSA (5'-GATC-CGGGATTACGATCGGGAGTCCCAGATTACGGCACCT-3'). The duplex oligonucleotides was incubated with each eluate after treatment with DUMSA as described in Material and Methods.

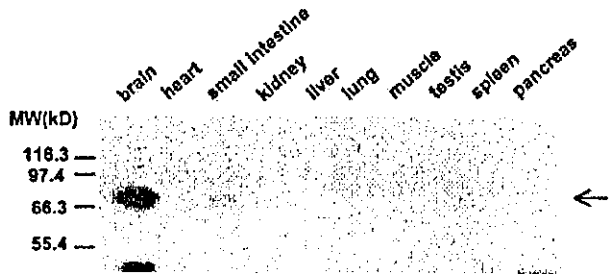

FIGURE 3 – Expression of hnRNP L in human tissues. Western blot analysis was carried out with anti-hnRNP L antibody. The membrane (INSTA-Blot) contains 10 μg per lane of different human tissue lysates. The arrow points to the hnRNP L protein.

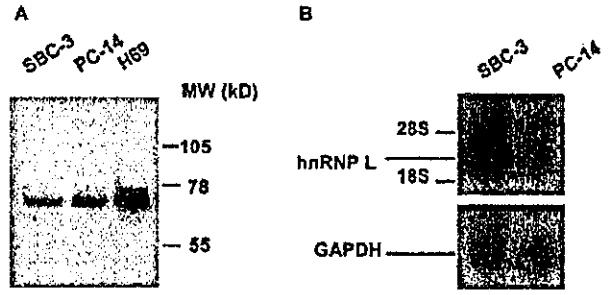

FIGURE 4 – Expression of hnRNP L in human lung cancer cell lines. (*a*) Cell lysates were prepared from 3 human lung cancer cell lines, separated with 7.5% SDS-PAGE, transferred to a membrane, and probed with anti-hnRNP L antibody. (*b*) Northern blotting was carried out with the 1030 bp fragment from hnRNP L cDNA as the probe.

room temperature, washed 3 times in TBST, incubated with anti-mouse IgG horseradish peroxidase antibody diluted (1:5000) in TBST with 1% skim milk for 1 hr at room temperature, and then washed 3 times in TBST. The signal was visualized with ECL (Amersham Pharmacia Biotech UK Ltd., Buckinghamshire, England), and Hyperfilm-MP (Amersham) was exposed to it.

Purification of DARP and amino acid sequencing

Purification of DARP was conducted as described previously.[9] DARP was detected by its ability to bind to DUMSA (one of DUMs)-DNA adduct in gel shift assays. Nuclear and cytoplasmic extracts from HeLa S3 cells (ATCC: American Type Culture Collection) were prepared according to previously published procedures. For identification of the DARP band, the aliquot of this material was subjected to DEAE-sephacel column again, and eluted with 0.5M stepwise procedure (0.1–0.5 M KCl) to give the small amount of purified DARP. Protein concentrations were estimated using Bio-Rad protein assay and the quality of the each fraction was checked by CBB (Coomassie brilliant blue) or silver staining of SDS-polyacrylamide gels. For analysis of amino acids sequence of DARP about 2 μg of affinity purified DARP was separated by 12% SDS-PAGE. The 60 kDa protein band was excised and digested with lysyl endopeptidase (WAKO, Japan) in 0.1 M Tris-HCl (pH 9.0), 4 M urea at 37°C for 16 hr. The resulting peptides were isolated by reversed phase HPLC on a RPC C2/C18 column (Amersham Pharmacia Biotech, Sweden). The amino acid sequence was determined by automated Edman degradation using a PPSQ-10 protein sequencer (Shimadzu, Japan).

Gel mobility shift assay

Labeled oligonucleotide (1 μg) was incubated with cell extract (final protein concentration, 20 μg/μl) at 30°C for 30 min in the presence of 2 μg of poly[dIdC]poly[dIdC] and 1 μg of BSA, except where stated, in a final volume of 15 μl of 0.1 M KCl HEDG. Where indicated, drug modified or unmodified calf thymus DNA was added to the reactions. Samples were electrophoresed in 6% polyacrylamide gel, dried and scanned.

Stable transfectants

Total RNA was prepared from HeLa cells with ISOGEN (Nippon Gene, Tokyo, Japan), and 14–784 and 636—1718 fragments of hnRNP L (2033 bp) were obtained by reverse transcription-polymerase chain reaction (RT-PCR). The PCR products were cloned in PCR II, a TA cloning plasmid vector, and then coupled at the Bcl I site. Subsequently, a fragment including hnRNP L was digested from the plasmid with Not I, and it was informed into the Not I site of the pRc/CMV vector. After confirming its sequence, this expression vector, pRc/CMV, containing cDNA of hnRNP L, was transfected into NIH3T3 cells with the Lipofectin reagent (Gibco BRL) according to the manufacturer's instructions. After 48 hr incubation, 1.5 mg/ml of G418 (Sigma) was added. Cells resistant to neomycin were selected, and isolated by limiting dilution methods.

Northern blotting

Total RNAs were prepared from SBC-3, PC-14 and NIH3T3 cells, and the 10 stable transfectants described above with ISO-

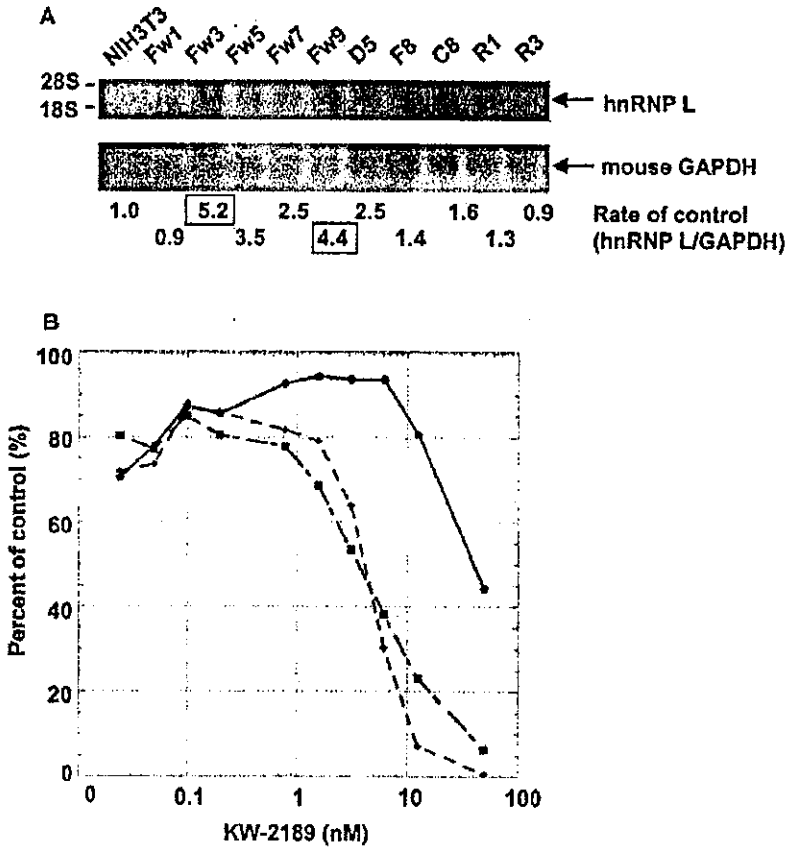

FIGURE 5 – Effect of hnRNP L on drug sensitivity. (*a*) Expression of hnRNP L mRNA in stable transfectants. Fw3 and Fw9 were chosen for the sensitivity tests. (*b*) MTT assay (KW-2189). C4 mock (●), Fw3 (■), Fw9 (□).

GEN reagent. RNA (12 μg) was electrophoresed and transferred to a positively charged nylon membrane (Hybond-N+). The 1030 bp fragment of hnRNP L cDNA was labeled with [α^{32}P]-dCTP by using the Rediprime II random primer labeling system (Amersham) and was used as a probe. The membrane was hybridized at 42°C overnight for blocking with sonicated salmon sperm DNA (Stratagene, La Jolla, CA) and hybridized at 42°C overnight with the labeled probe rotating. Washings were carried out in 2× SSC, 0.1% SDS, for 10 min at room temperature, 1× SSC, 0.1% SDS, for 1 hr at 42°C, and 0.2× SSC, 0.1% SDS, at 42°C for 1 hr. A BAS imaging plate (Fuji Photo Film Co. Ltd., Kanagawa, Japan) was exposed to the filter for 2 hr, and relative band intensities were measured with a BAS 2000 system (Fuji).

Growth-inhibition assay

The effect of hnRNP L on cell sensitivity to KW2189 was estimated by the 3-(4,5-dimethylthiazol-2yl)-2,5-diphenoyltetrazoliumbromide (MTT) assay. NIH3T3, and stable transfectants of hnRNP L cDNA, Fw3and Fw9 cells were exposed to 0–50 nM KW2189 for 72 hr before measuring absorbance. The OD values at 562–630 nm were measured with a 96-well microtiter plate reader, EL340 (Bio-Tek, Winooski, VT).

Immunochemical cell staining

Human lung cancer cell lines, SBC-3, PC-9, PC-14 and H69 cells were prepared on slide glasses with cytospin (Shandon, Pittsburgh, PA). The cells were dried and then fixed in cold acetone for 2 min. All of the incubation steps were carried out at room temperature, and Step 2 and 3 were carried out in the dark. The steps included: 1) incubation with 10% horse serum for 30 min for blocking; 2) incubation with anti-human hnRNP L (1:500 diluted in PBS with 1.5% blocking serum) for 60 min; and 3) incubation with fluorescence anti-mouse IgG (1:500 diluted) for 45 min. Slides were washed with 3 changes of PBS between each step. After Step 2 each washing was carried out for 5 min. The slides were mounted with 90% glycerol in PBS and examined with a fluorescence microscope (Nikon, Tokyo, Japan), equipped with fluorescein isothiocyanate filter set B-2A (Nikon).

EGFP-hnRNP L deletion mutants

pRc/CMV containing the 14–1718 fragment of hnRNP L cDNA (2033bp) was constructed as described above. After digesting the plasmid with SacII and BamHI, and the resulting fragment was introduced into the SacII/BamHI site of the pEGFP-C3 vector (Clontech, Palo Alto, CA), with the Takara DNA ligation system. Construction of deletion plasmids was carried out as follows. EGFP-hnRNP L (Construct 2) was partially digested with StuI and self-ligated to generate Constructs 3 and 6. PEGFP-hnRNP L was digested with BglII, and after extracting the 570 bp and 1023 bp fragments with a QIAquick Gel Extraction Kit (Qiagen, Hilden, Germany), each fragment was inserted into the BglII site of the pEGFP-C2 and -C3 vectors to generate Constructs 4 and 7, respectively. The 384 bp fragment of hnRNP L extracted by digesting with StuI was inserted into the SmaI site of pEGFP-C3 vectors to generate Construct 5. PEGFP-hnRNP L was digested with KpnI, and it self-ligated to generate Construct 8. The 584 bp fragment digested with KpnI and BglII and extracted was inserted into the BglII site of pEGFP-C3 vectors to generate Construct 9, and the 626 bp fragment digested with AccI was inserted into the AccI site of pEGFP-C3 vectors to generate Construct 10 (Fig. 1).

A cover-glass was placed on the bottom of each well of a 6-well culture dish, and each well was seeded with 1.6 × 10^5 NIH3T3 cells and incubated for 48 hr at 37°C. After diluting 2.5 μg/well of plasmid

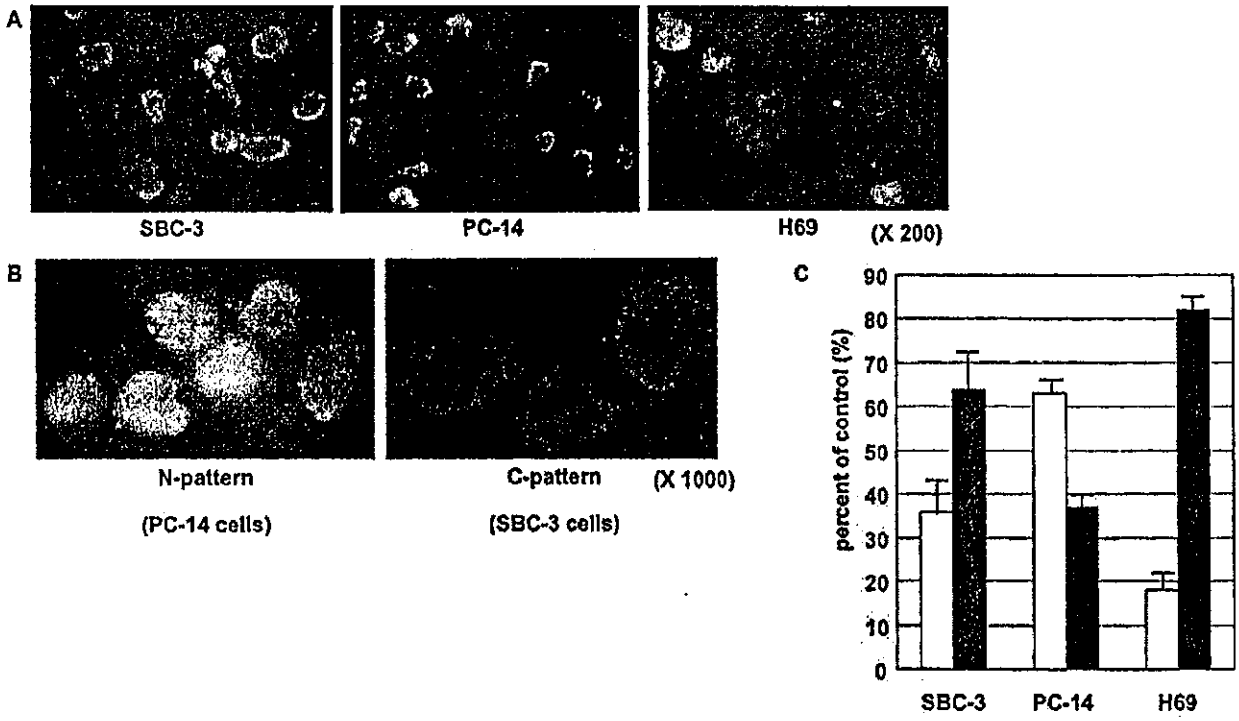

FIGURE 6 – Immunochemical staining of hnRNP L in human lung cancer cells. (*a*) Immunochemical cell staining was carried out using anti-hnRNP L antibody as the primary antibody and fluorescent anti-mouse IgG as the secondary antibody. (*b*) Intracellular localization of hnRNP L. (*c*) Cells were classified into N (white column) or C (gray column) patterns. Three independent cell counts were carried out.

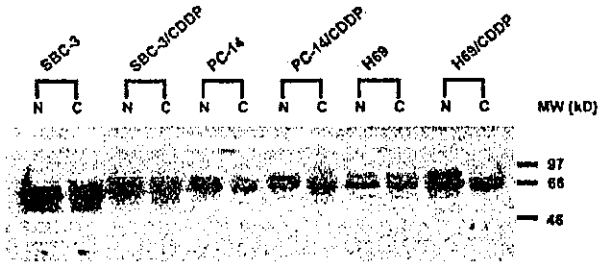

FIGURE 7 – Intracellular expression of hnRNP L in human lung cancer cell lines. The nuclear (N) and cytoplasmic (C) fractions of the cells were isolated as described in Material and Methods. Western blot analysis was carried out using anti-hnRNP L antibody. The cisplatin-resistant sublines were also examined to determine whether the localization patterns depended on the cell type.

DNA (pEGFP vectors containing deletion mutants of hnRNP L described above) in 1 ml/well of serum-free DMEM, 7.5 μl/well of 1 mM TransFast Reagent (Promega, Madison, WI) was added to the mixture. After allowing the mixture to stand for 15 min at room temperature, it was added to cells from which the growth medium was removed. The cells were then incubated for 1 hr at 37°C, and 1 ml/well of complete growth medium was added to them. At 24 hr after transfection, the cells were mounted on slides with aqueous mounting medium and examined under a fluorescence microscope (Nikon, B-2A filter, Tokyo, Japan).

RESULTS

Purification and sequence analysis of the DARP

Purification of the DARP was conducted as described previously.[9] After affinity purification, 2 main proteins were detected in SDS-PAGE with silver staining. Further purification efforts with DEAE-sephacel column chromatography gave a single band of Mr ~60,000 with the binding activity to the labeled duocarmycin-modified oligonucleotides (Fig. 2*a*). Coincubation of duocarmycin-treated calf thymus DNA with the labeled probe and purified DARP resulted in the retarded band in the gel mobility shift assay (Fig. 2*b*). Competition experiment in the presence of 30 and 300 ng of calf thymus DNA-DUMSA adduct demonstrated that 300 ng adduct reduced the intensity of the band in our previous study.[9]

The 60 kDa protein separated by SDS-PAGE was excised and digested with lysyl endopeptidase. The resulting peptides were eluted, separated by reversed phase HPLC, and sequenced. Three partial amino acid sequences were obtained, AAAGGGGGGGRYYGGG, DFSESRNNRFSTPEQAA and SDALETLGFLN, which were found to completely match parts of the predicted human heterogeneous nuclear ribonucleoprotein L. Gel mobility shift assay using anti-hnRNP L did not, however, show the supershift of the band induced by anti-hnRNP L (data not shown).

Expression of hnRNP L

Western blot analysis was carried out using a membrane containing normal human tissue lysates from different organs. A 68 kDa band of hnRNP L was detected in total protein extracts from brain and small intestine, but not in others, including normal lung (Fig. 3). The expression of hnRNP L protein, however, was detected in the human lung cancer cell lines (Fig. 4*a*). Northern blot analysis confirmed the expression of hnRNP L at the mRNA (~2 kbp) level in these cells (Fig. 4*b*). In contradiction to our first result that hnRNP L was not detected in normal lung tissue, the expression of hnRNP L in malignant cells seemed to increase.

Effect of hnRNP L on drug sensitivity

To evaluate the function of hnRNP L, hnRNP L cDNA was transfected into NIH3T3 cells, and stable transfectant clones were

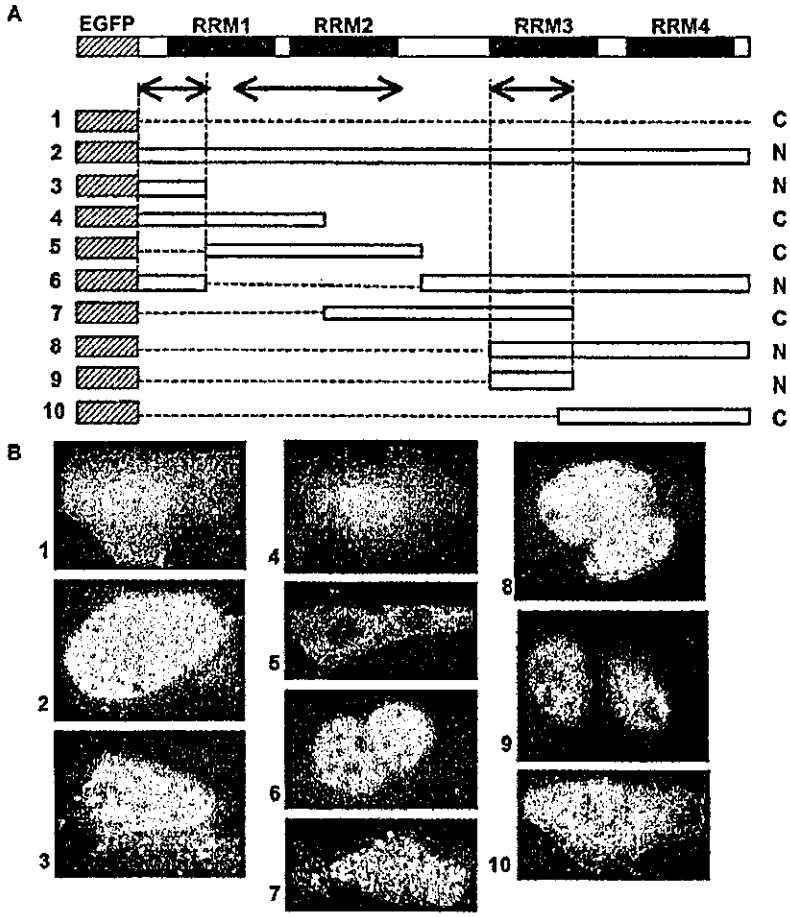

FIGURE 8 – Effect of hnRNP L deletion on the intracellular localization of EGFP-hnRNP L. (*a*) Arrows indicate the part expected to be responsible for localization of hnRNP L. Letters N (nuclear localization) and C (cytoplasmic localization) at the right end indicate the results of classification by the transfection study. (*b*) Localization of EGFP-hnRNP L deletion mutants. NIH3T3 cells were transfected with each construct, and they were examined by fluorescent microscopy to identify the localization of EGFP-fusion. The numbers correspond to those of the constructs in (*a*).

characterized. The Fw3 and Fw9 clones showed higher expression of hnRNP L mRNA than other transfectants by 5.2-fold and 4.4-fold to control respectively detected by Northern blot analysis (Fig. 5*a*).

We measured the growth inhibitory effect of KW-2189 in the hnRNP L transfectant cells by MTT assay. The IC_{50} values for KW-2189 in the Fw3 and Fw9 clones were 3.5 nM and 4.3 nM, respectively, and the Fw3 and Fw9 cells were 13.4-fold and 10.9-fold, respectively, more sensitive to KW-2189 than the Mock transfectant C4 cells (IC_{50}: 47 nM) (Fig. 5*b*). These results indicate that hnRNP L enhances cell sensitivity to the growth inhibitory effect of KW-2189 *in vitro*. We also examined the sensitivity of the transfectants to cisplatin and mitomycin C and no difference of the sensitivity was observed between the transfectants and the Mock cells (data not shown). The hnRNPs have been reported to regulate both nuclear and cytoplasmic events, as described above, and the intracellular localization of hnRNP L was examined in the next step to identify the site of action of hnRNP L in the sensitivity enhancement machinery.

Localization of hnRNP L protein in human lung cancer cell lines

We carried out immunofluorescence cell staining with anti-hnRNP L antibody to determine the subcellular localization of hnRNP L protein in human lung cancer cells (Fig. 6*a*). Based on the results, the localization of hnRNP L cells could be classified into two patterns: nuclear localization (N) and cytoplasmic localization (C) (Fig. 6*b*). As shown in Figure 6*c*, the cytoplasmic pattern was observed frequently in SBC-3 and H69 cells, whereas the nuclear pattern was common in PC-14 cells. To confirm this differential distribution, fractionated proteins from the nuclear and cytoplasmic fractions of these cells were immunoblotted with anti-hnRNP L antibody (Fig. 7). The results showed that hnRNP L was expressed equally in the nucleus and cytoplasm of the SBC-3 and H69 cells, whereas it was expressed predominantly in the nuclei of the PC-14 cells. These results are consistent with the immunocytological findings. In addition, the cisplatin-resistant sublines derived from these cells exhibited the same localization pattern as their parental cells. This indicates that the differential localization depends on the cell type.

Motifs required for the intracellular localization of hnRNP L

It has been reported that hnRNP L is localized in the nucleoplasm of HeLa cells, except the nucleoli,[12] but the mechanism of its localization remains unknown. To identify the motifs responsible for the localization of hnRNP L, we constructed an hnRNP L deletion series fused to EGFP (Fig. 8*a*), transfected the constructs into NIH3T3 cells, and examined them under a fluorescence microscope. As shown in Figure 8*b*, EGFP protein itself was rather evenly distributed throughout the cell, the cytoplasm and the nucleus (Transfectant 1). Full-length hnRNP L was present in the nucleoplasm, except the nucleoli (Transfectant 2). Deletion mutants containing the N-terminal portion of RRM1 or of RRM3 (Transfectants 3, 6, 8 and 9) showed hnRNP L localization in the nucleus. Transfectants 4, 5 and 7, containing the N-terminal portion of RRM2 showed hnRNP L distributed through the cell, whether they also contained that portion of RRM1 and RRM3 or not. In Transfectant 10, which lacked the N-terminal region of all

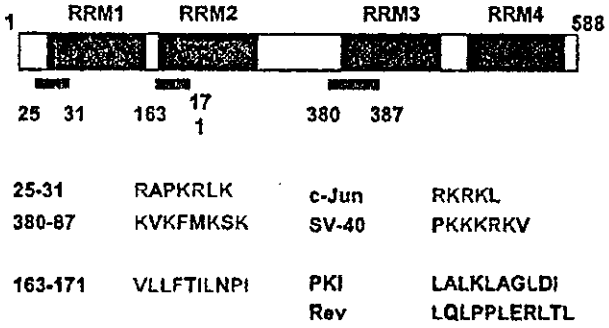

FIGURE 9 – NLS-like and NES-like sequences in hnRNP L. There are 2 NLS-like sequences that resemble the NLS sequences of c-Jun and SV-40 large T antigen and one NES-like sequence that resembles the NES sequences of PKI and Rev.

3 RRMs, hnRNP L was distributed throughout the cell. These results indicate that the N-terminal portion of each RRM is required for determination of the intracellular localization of hnRNP L (Fig. 8*a*, *arrows*). We then searched the sequence of hnRNP L and found 2 sequences that were rich in alkaline amino acids (residues 25–31, 380–387) and a sequence that was rich in hydrophobic amino acids (residue 163–171, Fig. 9). The sequences rich in alkaline amino acids showed high homology with the NLS sequences of c-Jun and SV40 large T antigen,[13,14] and the sequence rich in hydrophobic amino acids showed high homology with the NES sequences of PKI[15] and Rev[16] respectively. The N-terminal portion of RRM1 and RRM3 contain the NLS-like sequences, residue 25–31 and residue 380–387, respectively, and the N-terminal portion of RRM2 contains the NES-like sequence, residue 163–171.

DISCUSSION

There are approximately 20 major hnRNPs, and some of them have been reported to be highly expressed in cancer tissues. Sueoka *et al.*[3] demonstrated elevated expression of hnRNP B1 mRNA in human lung cancer tissue, and hnRNP I and hnRNP K mRNA have been reported in malignant glioblastoma and breast cancer, respectively.[2,17] We demonstrated expression of hnRNP L in human lung cancer cell lines and high expression of hnRNP L is presumably present in lung cancer tissue.

We reported previously that a nuclear protein in human cancer cells binds to the DUM-DNA adduct. The protein, DARP, preferentially bound to the DNA damage induced by DNA-alkylating minor groove binders such as DUMs and CC-1065. Because the amino acid sequence of DARP was identical to hnRNP L, hnRNP L is a candidate protein that binds to the DNA damage induced by DUM. A water-soluble derivative of DUM, KW-2189, exhibits broad spectrum antitumor activity in a series of experimental tumor models and entered clinical trials. KW-2189 was designed as a prodrug to generate active species, DU86, in tumor cells and DARP bounds to the DNA induced by DU86 (unpublished results). Although KW-2189 alkylates DNA *in vitro*, only the DU86-DNA adduct was detected in the human cells treated with KW-2189.[18,19] The transfection study demonstrated that hnRNP L enhanced the cellular sensitivity to KW2189. As described previously, DARP did not recognize the DNA adducts of cisplatin and mitomycin C *in vitro*.[18] We show that when we examined the transfectants for sensitivity to other DNA-damaging agents, *i.e.*, the major groove binders mitomycin C and cisplatin (data not shown), ectopic hnRNP L expression had no affect on cell sensitivity to them. These results suggest that DARP could be hnRNP L and it acts specifically on DNA damage induced by the minor groove binder.

Other possible mechanisms of increased sensitivity to KW-2189 are: 1) that hnRNP L facilitates transportation of the drug to the nucleus, and 2) that hnRNP L increases the stability of the drug-DNA adduct in a sequence-specific manner.

We have described the difference in intracellular localization of hnRNP L in human lung cancer cell lines. Although there is a report claiming that hnRNP L localized in the nucleoplasm in HeLa cells transfected with hnRNP L,[12] we showed that the intracellular localization of hnRNP L differs among human lung cancer cell lines.

There was a report that hnRNP A2 is located in the cytoplasm in post-mitotic phase.[20] In this study, few mitotic cells were observed in the culture condition indicating that mitosis was not correlated with hnRNP L distribution. We speculate that in the case of hnRNP A2 a different mechanism might be involved in the intracellular localization of hnRNP L. Nevertheless, synchronization experiments must be examined.

SBC-3 and PC-14 cells grow faster than H69 cells. Even though cell growths of SBC-3 and PC-14 cells were equal in our culture condition, distribution of hnRNP L in these cells were different. This result indicate that the distribution depends on the cell type rather than difference of the cell growth.

To determine whether the localization of hnRNP L is altered by drug exposure, we examined the immunofluorescent staining of hnRNP L in lung cancer cells exposed to KW-2189 for 24 hr. An increased population of cells in which hnRNP L was localized in the nucleus was observed after exposure of a small cell lung cancer (SBC-3) cell line to KW-2189 (data not shown). Although this result was not observed in the rest two cell lines, it can support the hypothesis that hnRNP L helps drugs to transport into nuclear and involves in cell sensitivity mentioned above.

To test the hypothesis that the differences in intracellular localization in lung cancer cells are due to gene alterations, we compared the hnRNP L cDNA sequences in these cell lines. No mutations were detected in any of the lines (data not shown), suggesting that hnRNP L might be co-localized with other proteins. Interaction between hnRNPs has been reported and hnRNP L is known to have a binding domain for interaction with other hnRNPs (*e.g.*, hnRNP I and hnRNP K),[21] which are recognized to have NLS. Based on this evidence, the differences in localization of hnRNP L in these cell lines might be due to changes in the molecules that interact with hnRNP L, such as hnRNP I or K. In addition, the putative sites for regulation of localization signal in hnRNP L that we found (25–31, 380–387 and 163–171) would be involved in these interactions. Further studies should extend the potential use of hnRNP L as a factor to assess sensitivity to chemotherapy and candidate molecules for drug development. In addition, expression of hnRNP L needs to be investigated in tissue from lung cancer patients for therapeutic exploitation.

In summary, we have demonstrated the expression of hnRNP L with different intracellular localization in human lung cancer cell lines and that ectopic hnRNP L expression increases cellular sensitivity to a minor groove binder.

ACKNOWLEDGEMENT

The authors are grateful to Dr. G. Dreyfuss for providing anti-hnRNP L antibody.

REFERENCES

1. Dreyfuss G, Matunis MJ, Pinol-Roma S, Burd CG. hnRNP proteins and the biogenesis of mRNA. Annu Rev Biochem 1993;62:289–321.
2. Jin W, McCutcheon IE, Fuller GN, Huang ES, Cote GJ. Fibroblast growth factor receptor-1 α-exon exclusion and polypyrimidine tract-binding protein in glioblastoma multiforme tumors. Cancer Res 2000; 60:1221–4.

3. Sueoka E, Goto Y, Sueoka N, Kai Y, Kozu T, Fujiki H. Heterogeneous nuclear ribonucleoprotein B1 as a new marker of early detection for human lung cancers. Cancer Res 1999;59:1404–7.
4. Shih SC, Claffey KP. Regulation of human vascular endothelial growth factor mRNA stability in hypoxia by heterogeneous nuclear ribonucleoprotein L. J Biol Chem 1999;274:1359–65.
5. Liu X, Mertz JE. HnRNP L binds a *cis*-acting RNA sequence element that enables intron-dependent gene expression. Genes Dev 1995;9: 1766–80.
6. Ogasawara H, Nishio K, Takeda Y, Ohmori T, Kubota N, Funayama Y, Ohira T, Kuraishi Y, Isogai Y, Saijo N. A novel antitumor antibiotic, KW-2189 is activated by carboxyl esterase and induces DNA strand breaks in human small cell lung cancer cells. Jpn J Cancer Res 1994;85:418–25.
7. Ogasawara H, Nishio K, Kanzawa F, Lee YS, Funayama Y, Ohira T, Kuraishi Y, Isogai Y, Saijo N. Intracellular carboxyl esterase activity is a determinant of cellular sensitivity to the antineoplastic agent KW-2189 in cell lines resistant to cisplatin and CPT-11. Jpn J Cancer Res 1995;86:124–9.
8. Ogasawara H, Nishio K, Ishida T, Arioka H, Fukuoka K, Saijo N. *In vitro* enhancement of antitumor activity of a water-soluble duocarmycin derivative, KW-2189, by caffeine-mediated DNA-repair inhibition in human lung cancer cells. Jpn J Cancer Res 1997;88:1033–7.
9. Asai A, Yano K, Mizukami T, Nakano H. Characterization of a duocarmycin-DNA adduct-recognizing protein in cancer cells. Cancer Res 1999;59:5417–20.
10. Kasahara K, Fujiwara Y, Nishio K, Ohmori T, Sugimoto Y, Komiya K, Matsuda T, Saijo N. Metallothionein content correlates with the sensitivity of human small cell lung cancer cell lines to cisplatin. Cancer Res 1991;51:3237–42.
11. Ohmori T, Morikage T, Sugimoto Y, Fujiwara Y, Kasahara K, Nishio K, Ohta S, Sasaki Y, Takahashi T, Saijo N. The mechanism of the difference in cellular uptake of platinum derivatives in non-small cell lung cancer cell line (PC-14) and its cisplatin-resistant subline (PC-14/CDDP). Jpn J Cancer Res 1993;84:83–92.
12. Hahm B, Cho OH, Kim JE, Kim YK, Kim JH, Oh YL, Jang SK. Polypyrimidine tract-binding protein interacts with HnRNP L. FEBS Lett 1998;425:401–6.
13. Kalderon D, Richardson WD, Markham AF, Smith AE. Sequence requirements for nuclear location of simian virus 40 large-T antigen. Nature 1984;311:33–8.
14. Lanford RE, Butel JS. Construction and characterization of an SV40 mutant defective in nuclear transport of T antigen. Cell 1984;37:801–13.
15. Wen W, Meinkoth JL, Tsien RY, Taylor SS. Identification of a signal for rapid export of proteins from the nucleus. Cell 1995;82:463–73.
16. Fischer U, Huber J, Boelens WC, Mattaj IW, Luhrmann R. The HIV-1 Rev activation domain is a nuclear export signal that accesses an export pathway used by specific cellular RNAs. Cell 1995;82:475–83.
17. Mandal M, Vadlamudi R, Nguyen D, Wang RA, Costa L, Bagheri-Yarmand R, Mendelsohn J, Kumar R. Growth factors regulate heterogeneous nuclear ribonucleoprotein K expression and function. J Biol Chem 2001;276:9699–704.
18. Asai A, Nagamura S, Saito H, Takahashi I, Nakano H. The reversible DNA-alkylating activity of duocarmycin and its analogues. Nucleic Acids Res 1994;22:88–93.
19. Okamoto A, Asai A, Saito H, Okabe M, Gomi K. Differential effect of duocarmycin A and its novel derivative DU-86 on DNA strand breaks in HeLa S3 cells. Jpn J Cancer Res 1994;85:1304–11.
20. Kim JH, Hahm B, Kim YK, Choi M, Jang SK. Protein-protein interaction among hnRNPs shuttling between nucleus and cytoplasm. J Mol Biol 2000;298:395–405.
21. Kamma H, Satoh H, Matusi M, Wu WW, Fujiwara M, Horiguchi H. Characterization of hnRNP A2 and B1 using monoclonal antibodies: intracellular distribution and metabolism through cell cycle. Immunol Lett 2001;76:49–54.

Int. J. Cancer: 108, 464–472 (2004)

Publication of the International Union Against Cancer

SYNERGISTIC INTERACTION BETWEEN THE EGFR TYROSINE KINASE INHIBITOR GEFITINIB ("IRESSA") AND THE DNA TOPOISOMERASE I INHIBITOR CPT-11 (IRINOTECAN) IN HUMAN COLORECTAL CANCER CELLS

Fumiaki KOIZUMI[1], Fumihiko KANZAWA[3], Yutaka UEDA[1], Yasuhiro KOH[3], Shoji TSUKIYAMA[3], Fumiko TAGUCHI[1,3], Tomohide TAMURA[2], Nagahiro SAIJO[2] and Kazuto NISHIO[1,3]*

[1]*Support Facility of Project Ward, National Cancer Center Hospital, Tokyo, Japan*
[2]*Medical Oncology, National Cancer Center Hospital, Tokyo, Japan*
[3]*Pharmacology Division, National Cancer Center Research Institute, Tokyo, Japan*

Epidermal growth factor receptor [EGFR (HER1, erbB1)] is a receptor with associated tyrosine kinase activity, and is expressed in colorectal cancers and many other solid tumors. We examined the effect of the selective EGFR tyrosine kinase inhibitor (EGFR-TKI) gefitinib ("Iressa") in combination with the DNA topoisomerase I inhibitor CPT-11 (irinotecan) on human colorectal cancer cells. EGFR mRNA and protein expression were detected by RT-PCR and immunoblotting in all 7 colorectal cancer cell lines studied. Gefitinib inhibited the cell growth of the cancer cell lines *in vitro* with an IC_{50} range of 1.2–160 μM by 3,(4,5-dimethyl-2-thiazolyl)-2,5-diphenyl-2H-tetrazolium bromide (MTT) assay. Lovo cells exhibited the highest level of protein and autophosphorylation of EGFR and were the most sensitive to gefitinib. The combination of gefitinib and CPT-11 induced supra-additive inhibitory effects in COLO320DM, WiDR and Lovo cells, assessed by an *in vitro* MTT assay. Administration of gefitinib and CPT-11 had a supra-additive inhibitory effect on WiDR cells and tumor shrinkage was observed in Lovo cell xenografts established in nude mice, whereas no additive effect of combination therapy was observed in COLO320DM cells. To elucidate the mechanisms of synergistic effects, the effect of CPT-11-exposure on phosphorylation of EGFR was examined by immunoprecipitation. CPT-11 increased phosphorylation of EGFR in Lovo and WiDR cells in time- and dose-dependent manners. This EGFR activation was completely inhibited by 5 μM gefitinib and gefitinib-induced apoptosis was enhanced by combination with CPT-11, measured by PARP activation although no PARP activation was induced by 5 μM CPT-11 alone. These results suggested that these modification of EGFR by CPT-11, in Lovo cells, is a possible mechanism for the synergistic effect of CPT-11 and gefitinib. These findings imply that the EGFR-TKI gefitinib and CPT-11 will be effective against colorectal tumor cells that express high levels of EGFR, and support clinical evaluation of gefitinib in combination with CPT-11, in the treatment of colorectal cancers.

Key words: *combination; gefitinib; "Iressa"; colorectal cancer; irinotecan*

Colorectal cancer is a major public health concern. Although chemotherapy appears to be of very limited value in advanced colorectal cancer, there have been many efforts to apply combination chemotherapy in patients with primary disease.[1–3]

The combination of fluorouracil and leucovorin used to be recognized as standard therapy for colorectal cancer, but the topoisomerase I inhibitor, irinotecan (CPT-11), has recently been demonstrated to be active against colorectal cancer that was resistant to prior therapy.[4,5] Moreover, the CPT-11/5-FU/LV combination has been approved as standard chemotherapy by the US FDA for metastatic colorectal cancer.[6] However, patients treated with CPT-11 plus bolus 5-FU/leucovorin have been found to have a 3-fold higher rate of treatment-induced or treatment-exacerbated death than patients treated with other arms of the respective studies.[7] We have therefore been seeking a new combination regimen containing CPT-11 and target-based drugs.

The development of target-based drugs, including receptor tyrosine kinase inhibitors (TKI), is one of the promising strategies for cancer chemotherapy.[8,9] Colorectal cancers express receptors of the type 1 tyrosine kinase family, including epidermal growth factor receptor (EGFR) and c-erbB-2,[10–12] and the EGFR has emerged as a central molecular target for modulation in cancer therapeutics. The correlation between high expression of EGFR and clinically aggressive malignant disease has made EGFR a promising target of therapy for many epithelial tumors, which represent approximately 2/3 of all human cancers. In solid cancers, including colorectal cancers, high EGFR expression correlates with poor prognosis.[11] Gefitinib ("Iressa") is an orally active, selective EGFR-TKI that blocks signal transduction pathways involved in the proliferation and survival of cancer cells and in other host-dependent processes promoting cancer growth.[13,14] In EGFR tyrosine kinase assays, gefitinib has an IC_{50} of 0.033 μM. Inhibition of c-erbB-2 and KDR occurs at doses 100-fold higher than for EGFR inhibition.[15] We have previously demonstrated that gefitinib exerts high growth-inhibitory activity against EGFR-positive tumors in a xenograft model,[16] and gefitinib is therefore expected to be a potent therapeutic agent against EGFR-positive colorectal cancers. In recent years, it has been shown that the combined treatment of established human colorectal cancer xenograft with anti-EGFR drug (cetuximab or gefitinib) and with topoisomerase I inhibitor, topotecan, increase the antitumor activity of these drugs.[17,18] The aim of the present study was to investigate the combination effect of gefitinib and CPT-11 and to elucidate the biochemical mechanism of synergistic interaction in colorectal cancers.

MATERIAL AND METHODS

Drugs and chemicals

Gefitinib (N-(3-chloro-4-fluorophenyl)-7-methoxy-6-[3-(morpholin-4-yl)propoxy] quinazolin-4-amine) was provided by AstraZeneca (Cheshire, UK). Gefitinib was dissolved in dimethyl sulfoxide (DMSO) for the *in vitro* study and suspended in 5% glucose, pH 6, for the *in vivo* study. CPT-11 was obtained from Yakult Honsha (Tokyo, Japan). CPT-11 was dissolved in 45 mg/ml solvitol (pH 3-4) for both the *in vivo* and *in vitro* studies.

*Correspondence to: Support Facility of Project Ward, National Cancer Center Hospital, 5-1-1 Tsukiji, Chuo-ku, Tokyo, 104-0045, Japan. Fax: +81-3-3547-5185. E-mail: knishio@gan2.res.ncc.go.jp

Received 19 May 2003; Revised 2 August 2002; Accepted 22 August 2003

DOI 10.1002/ijc.11539

Animals

Female BALB/c nude mice, 6-weeks-old, were purchased from Japan Charles River Co., Ltd. (Atsugi, Japan). All mice were maintained in our laboratory under specific-pathogen-free conditions.

Cells and culture

Human colorectal cancer cell lines WiDR, LS-174T, COLO320DM, COLO320HSR, Lovo, SW480 and HCT116 were obtained from ATCC (Lockville, MD). Lovo cells, SW480 and HCT116 cells were maintained in HAM's F12 medium (GIBCO BRL, Grand Island, NY), Leibovitz's L-15 medium and McCoy's 5A medium (GIBCO BRL), respectively, all supplemented with 10% heat-inactivated fetal bovine serum (FBS). Other cell lines were maintained in RPMI1640 (Nikken Bio Med. Lab., Kyoto, Japan) supplemented with 10% FBS.

Growth-inhibition assay

We used the tetrazolium dye [3,(4,5-dimethyl-2-thiazolyl)-2,5-diphenyl-2H-tetrazolium bromide, MTT] assay to evaluate the cytotoxicity of various drug concentrations. A 200 ml volume of an exponentially growing cell suspension (5×10^3–1.5×10^4 cells/ml) was seeded into a 96-well microtiter plate and 20 μl of each drug at various concentrations was added. After incubation for 72 hr at 37°C, 20 μl of MTT solution (5 mg/ml in phosphate buffered saline, PBS) was added to each well and the plates were incubated for a further 4 hr at 37°C. After centrifuging the plates at 200*g* for 5 min, the medium was aspirated from each well, and 180 μl of DMSO was added to each well to dissolve the formazan. Optical density was measured at 562 and 630 nm with a Delta Soft ELISA analysis program interfaced with a Bio-Tek Microplate Reader (EL-340, Bio-Metallics, Princeton, NJ). Each experiment was performed in 6 replicate wells for each drug concentration and carried out independently 3 or 4 times. The IC_{50} value was defined as the concentration needed for a 50% reduction in the absorbance calculated based on the survival curves. Percent survival was calculated as follows: (mean absorbance of 6 replicate wells containing drugs − mean absorbance of 6 replicate background wells)/(mean absorbance of 6 replicate drug-free wells − mean absorbance of 6 replicate background wells) × 100.

RT-PCR

Specific primers designed for EGFR CDS were used for detection of EGFR mRNA as described elsewhere.[16] First-strand cDNA was synthesized from the cells' RNA with an RNA PCR Kit (TaKaRa Biomedicals, Ohtsu, Japan). After reverse transcription of 1 μg of total RNA with Oligo(dT)-M4 adaptor primer, the whole mixture was used for PCR with 2 oligonucleotide primers (5′-AATGTGAGCAGAGGCAGGGA-3′,5′GGCTTGGTTTG-GAGCTTCTC-3′). PCR was performed with initial denaturation at 94°C for 2 min, 25 cycles of amplification (denaturation at 94°C for 30 sec, annealing at 55°C for 60 sec and extension at 72°C for 105 sec).

Immunoprecipitation and immunoblotting

The cultured cells were washed twice with ice-cold PBS, lysed in EBC buffer (50 mM Tris-HCl, pH 8.0, 120 mM NaCl, 0.5% Nonidet P-40, 100 mM NaF, 200 mM Na orthovanadate and 10 mg/ml each of leupeptin, aprotinin and phenylmethylsulfonyl fluoride). The lysate was cleared by centrifugation at 20,000*g* for 5 min, and the protein concentration of the supernatant was measured by BCA protein assay (Pierce, Rockford, IL). For Immunoblotting, 20 μg samples of protein were electrophoretically separated on a 7.5% SDS-polyacrylamide gel and transferred to a polyvinylidene difluoride (PVDF) membrane (Millipore, Bedford, MA). The membrane was probed with rabbit polyclonal antibody against EGFR (1005; Santa Cruz Biotech, Santa Cruz, CA), HER2/neu (c-18; Santa Cruz), phospho-EGFR specific for Tyr 845, Tyr 1045, and Tyr 1068 (numbers 2231, 2235 and 2234; Cell Signaling, Beverly, MA) and cleaved PARP (number 9544; Cell Signaling) as the first antibody, followed by horseradish peroxidase-conjugated secondary antibody. The bands were visualized by electrochemiluminescence (ECL, Amersham, Piscataway, NJ). For immunoprecipitation, 5×10^6 cells were washed, lysed in EBC buffer, and centrifuged. The resultant supernatants (1,500 μg) were incubated with the anti-EGFR antibody (1005) at 4°C overnight. The immunocomplex were absorbed onto protein A/G-Sepharose beads, washed 5 times with lysate buffer, denatured and subjected to electrophoresis on a 7.5% polyacrylamide gel followed by immunostaining probed with antiphosphotyrosine antibody (PY-20, BD Bioscience Clontech, Tokyo, Japan).

Combined effect of gefitinib and CPT-11 in vitro

The combined effect of gefitinib and CPT-11 on colorectal cancer cell growth was evaluated by the combination index (CI) analysis method.[6] For any given drug combination, CI represents the degree of synergy, additivity or antagonism. CI was expressed in terms of fraction-affected (F_a) values, which represents the percentage of cells killed or inhibited by the drug. Using the mutually exclusive ($\alpha=0$) or mutually nonexclusive ($\alpha=1$) isobologram equation, the F_a/CI plots for each cell line was constructed by computer analysis of the data generated from the median effect analysis. CI values were interpreted as follows: <1.0 = synergism; 1.0 = additive and >1.0 = antagonism.

Using the median-effect method, developed by Chou and Talalay, the dose-response curve was plotted for each drug and for multiple doses of a fixed-ratio combination by using the equation:

$$f_a/f_u = (D/D_m)^m ,$$

where, D is the dose-administered, Dm is the dose required for 50% inhibition of growth, f_a is the fraction affected by dose D, f_u is the unaffected fraction and m is a coefffect curve. The dose-response curve was plotted by logarithmic conversion of the equation to determine the m and D_m values, and the dose D_x required for x percent effect $(f_a)_x$ was then calculated as

$$D_x = D_m[f_a]_x/(f_u)x]^{1/m} .$$

Thus, CI can be defined by the isobologram equation

$$CI = (D)_1/(D_x)^1 + (D)_2/(D_x)2 + \alpha(D)_1(D)_2/(D_x)_1(D_x)_2 ,$$

where $(D_x)_1$ is the dose of Drug-1 required to produce x percent effect alone, and $(D)_1$ is the dose of Drug 1 required to produce the same x percent effect in combination with Drug 2; similarly, $(Dx)_2$ is the dose of Drug 2 required to produce x percent effect alone and $(D)_2$ is the dose of Drug 2 required to produce the same x percent effect in combination with Drug 1. Theoretically, CI is the ratio of the combined dose to the sum of the single-drug doses at an isoeffective level. Consequently, CI values <1 indicate synergism, values >1 indicate antagonism and a value of 1 indicates additive effects. The CI values obtained from both the classical nonconservative ($\alpha=0$) and conservative ($\alpha=1$) isobologram equations are presented in this report.

Growth-inhibition assay in vivo

Experiments were performed in accordance with the United Kingdom Coordinating Committee on Cancer Research Guidelines for the welfare of animals in experimental neoplasia (second edition).

In vivo experiments were scheduled to evaluate the combined therapeutic effect on preexisting tumors of oral or intraperitoneal administration of gefitinib and intravenous injection of CPT-11. The dose of each drug was set based on the results of a preliminary experiment involving administration of each drug alone. Ten days before administration, 1×10^7 WiDR and COLO320DM or 2×10^6 Lovo cells were injected subcutaneously into the back of mice. Five or 6 mice per group were injected with tumor cells. Tumor bearing mice were either given gefitinib, 40 mg/kg/day *p.o.* on days 1–10, or CPT-11, 40 mg/kg/day *i.v.* on days 1, 5 and 9, or

both, or placebo (5%(w/v) glucose solution). Alternatively, gefitinib, 30 or 60 mg/kg, *i.p.* days 1–14, and *i.v.* CPT-11, 16.7 or 33.3 mg/kg, *i.v.* on days 1, 5 and 9, were administered to the mice. Tumor diameters were measured with calipers on days 1, 4, 7, 10, 14, 18 and 22 to evaluate the effects of treatment, and tumor volume was determined by using the following equation: tumor volume = $ab^2/2$ (mm^3) (where a is the largest diameter of the tumor and b is the shortest diameter). Day "x" denotes the day on which the effect of the drugs was estimated, and day "0" denotes the first day of treatment. All mice were sacrificed on day 22 after measuring their tumors.

Statistical analysis

Differences between the test groups were analyzed by 1-factor ANOVA followed by Fisher's protected least significant difference (PLSD). A value of $p<0.05$ was considered statistically significant.

RESULTS

EGFR and HER2 expression and EGFR autophsophorylation in colorectal cancer cells

We examined EGFR mRNA expression by RT-PCR analysis using 2 specific primers. Approximately 570 bp-long PCR products were amplified in all cell lines that exhibited expression of EGFR mRNA (Fig. 1*a*). Comparison of the protein expression levels of EGFR in colorectal cancer cells by immunoblotting (Fig. 1*b*) revealed high expression in Lovo and WiDR cells. EGFR protein was also detected in LS-174T, COLO320DM, COLO320HSR, HCT116 and SW480 cells, although the expression levels in COLO320DM and COLO320HSR are subtle. The highest expression level of phosphrylated EGFR measured by phospho-specific EGFR antibody (Tyr845, Tyr1045 and Tyr1068) was observed in Lovo cells (Fig. 1*b*). Because the function of EGFR is closely related to that of other HER families including HER2/neu, we also examined the protein level of HER2/neu. High expression of HER2/neu were observed in LS-174T, HCT-116 and SW480 (Fig. 1*b*).

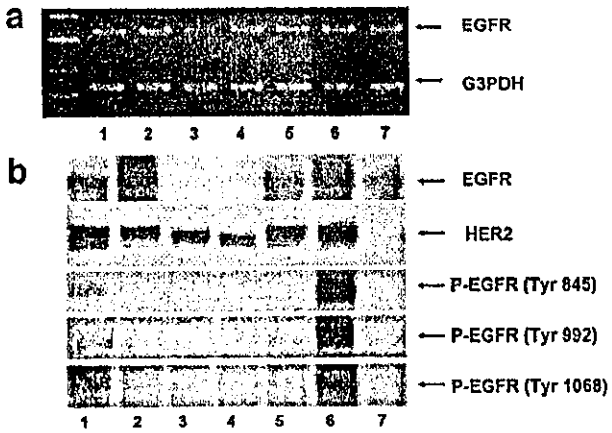

FIGURE 1 – EGFR expression in colorectal cancer cells. (*a*) Expression of EGFR mRNA in each cell line was detected by RT-PCR using specific primers designed for EGFR CDS. Expression of G3PDH mRNA was detected. Twenty-five cycles of PCR amplification were performed for each PCR product. Lanes 1–7 represent LS-174T, WiDR, COLO320DM, COLO320HSR, HCT116, Lovo and SW480 cells, respectively. (*b*) A 20 μg sample of total cell lysates was separated by 7.5% SDS-PAGE, transferred to PVDF membrane, and incubated with a specific anti-human EGFR, HER2/neu and phospho-EGFR (Tyr845, Tyr992 and Tyr1068).

Cellular sensitivity of colorectal cancer cells to gefitinib and CPT-11

The growth inhibitory effect of gefitinib and CPT-11 on colorectal cancer cells was examined by MTT assay. The IC_{50} values of gefitinib for the cell lines ranged from 1.2 μM (Lovo cells) to 160 μM (HCT116 cells) (Table I). No significant relationship was observed between EGFR expression levels and IC_{50} values among these cell lines. However, Lovo cells, which exhibited the highest EGFR expression and its phosphorylation, were the most sensitive to gefitinib. On the other hand, the IC_{50} values of CPT-11 for the cell lines ranged from 5.2 μM (Lovo) to 35 μM (SW480). The range of sensitivity to gefitinib was wider than to CPT-11.

In vitro *combined effect of gefitinib and CPT-11 on colorectal cancer cell lines*

Based on the results of the evaluation of *in vitro* growth-inhibition, 4 cell lines (WiDR, COLO320DM, Lovo, and SW480 cells) were selected for the *in vitro* combination study. Cells were treated with gefitinib or CPT-11 alone or in concomitant combination at fixed molar ratio for 72 hr. The ratios of gefitinib and CPT-11 were set based on the IC_{50} values of each cell line. Growth rate values are averages of data from at least 3 independent experiments. The effects of combinations of gefitinib and CPT-11 on cell growth are shown in Figure 2. CI values of <1, >1 and 1 indicate a supra-additive effect (synergism), antagonistic effect and additive effect, respectively. A low CI index was observed in WiDR, COLO320DM and Lovo cells over a wide range of inhibition levels. Synergistic effects were also observed in the relatively high F_a values in SW480 cells. These results suggest that gefitinib and CPT-11 had a synergistic effect on most of the colorectal cancer cell lines *in vitro*.

In vivo *combination effects of gefitinib and CPT-11*

In order to determine whether the combination of these 2 drugs is also synergistic against colorectal cancer *in vivo*, the growth-inhibitory effect of the combination was evaluated against the colorectal cancer cells in tumor xenografts. The growth inhibitory effect of gefitinib, 30 mg/kg, *i.p.* days 1–10, and CPT-11, 40 mg/kg, *i.v.* days 1, 5 and 9, on WiDR cells was evaluated (Fig. 3*a*,*b*). Administration of gefitinib or CPT-11 alone suppressed the tumor volume of WiDR cells with a T/C value of 73.9% and 69.2%, respectively, at day 22, (Fig. 3*c*), whereas gefitinib+CPT-11 suppressed WiDR tumors with T/C value of 51.8% at day 22, but this was not statistically significant (Fig. 3*d*, $p=0.164$ by 1-factor ANOVA). A 10% body weight loss was observed until day 15 in mice given the combination, but body weight recovered by day 22 (Fig. 3*e*). No growth inhibitory effect of single or combined therapy of CPT-11 and gefitinib in COLO320DM cells were observed (data not shown). In mice transplanted with Lovo cells, with a high EGFR expression level, marked tumor growth inhibition was achieved with gefitinib+CPT-11 (Fig. 3*f*). The T/C of the combination schedule at day 11 was 22.8% and significantly lower than in the control ($p<0.0012$ by Fisher's PSLD, Fig. 3*g*). A 10% maximum body weight loss until day 15 was also observed in mice treated with the combination (Fig. 3*j*).

Alternatively, the combined effect of oral administration of gefitinib and intravenous administration of CPT-11 was evaluated in mice transplanted with Lovo cells. Gefitinib, 30 or 60 mg/kg *p.o.* days 1–14, and CPT-11, 16.7 or 33.3 mg/kg *i.v.* days 1, 5 and 9, were administered (schedule 2, Fig. 4*a*), and greater growth inhibition was observed in mice treated with this combination, compared to the controls (Fig. 4*b*) A more marked growth-inhibitory effect was observed at a higher dose of CPT-11 (16.7 *vs.* 33.3 mg/kg), but there was no difference between 30 mg/kg and 60 mg/kg of gefitinib in the combination. The combination of gefitinib (30 and 60 mg/kg) and CPT-11 (33.3 mg/kg/*i.v.*) resulted in tumor reduction during treatment that was significant at day 15 (Fig. 4*c*). The T/C values imme-

TABLE I – *IN VITRO* GROWTH-INHIBITORY ACTIVITY OF GEFITINIB AND CPT-11 IN HUMAN COLORECTAL CANCER CELLS (MTT ASSAY)[1]

Cell line	gefitinib		CPT-11	
	IC_{50} (μM)	Concentration range (μM)	IC_{50} (μM)	Concentration range (μM)
WiDR	10 ± 1.1	0.83–53	33 ± 7.5	1.6–160
LS-174T	100.4 ± 10.1	N.D.	13	N.D.
COLO320DM	11 ± 3.8	0.63–100	11 ± 0.6	1.6–160
COLO320HSR	22	N.D.	5.5	N.D.
HCT116	177.0 ± 12.2	N.D.	11	N.D.
SW480	23 ± 0.6	1.6–10	35 ± 5.5	1.6–50
Lovo	1.2 ± 0.59	0.31–25	5.2 ± 0.82	0.16–10

[1]The IC_{50} value (μM) of each drug was measured by MTT assay, as described in the Materials and Methods. Each value is a mean ± SD of 3 or 4 independent experiments–N.D., not determined.

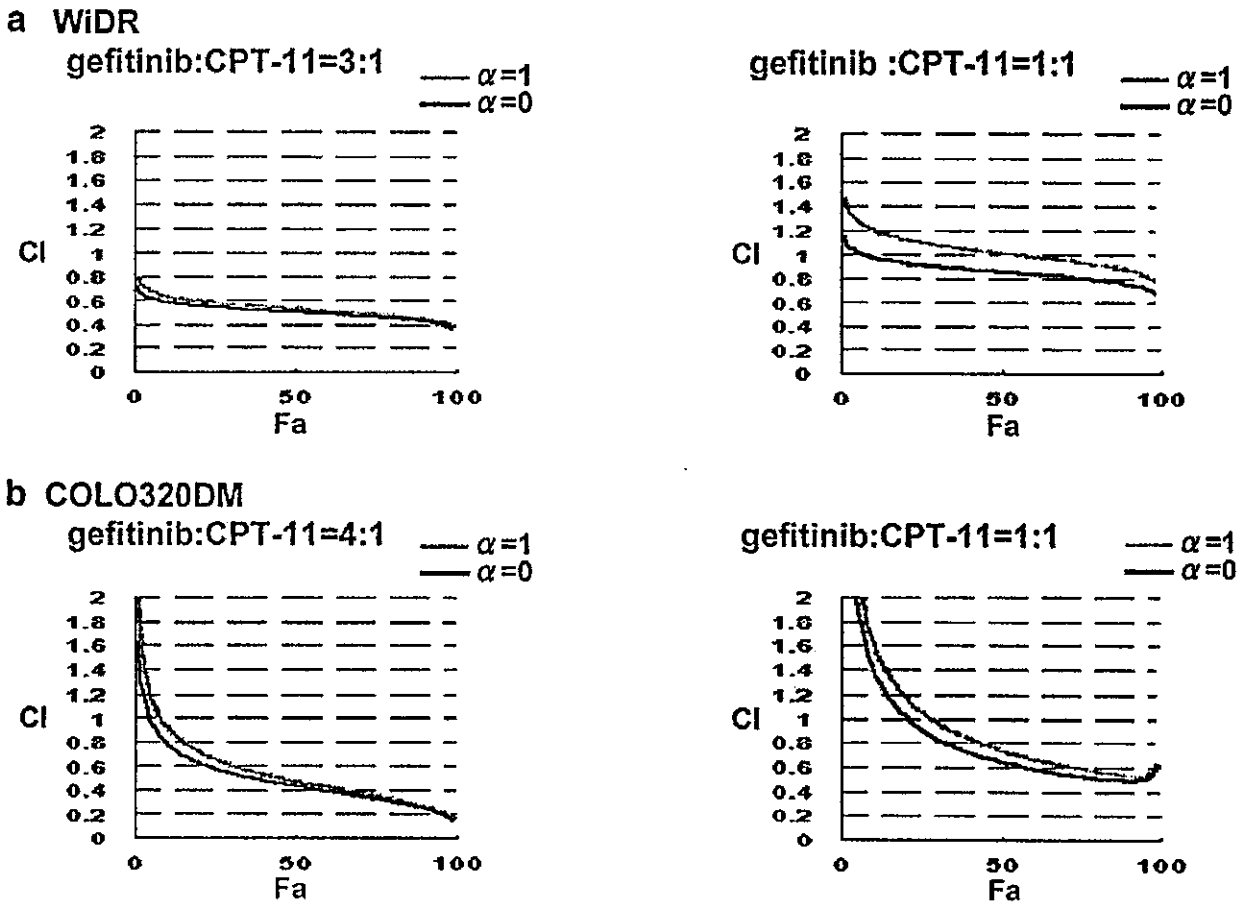

FIGURE 2 – Combination index (CI) plots of interactions between gefitinib and CPT-11. Cells were treated with gefitinib and CPT-11 alone and in combination at fixed molar ratios (molar ratios of gefitinib to CPT-11 of 3:1 and 1:1 [(*a*) WiDR], 4:1 and 1:1 [(*b*) COLO320DM], 1:2 and 1:5 [(*c*) Lovo], 1:1 [(d) SW480]. Using the mutually exclusive (CI) or mutually nonexclusive (CI') isobologram equation, the affected fraction (F_a)-CI plot for each cell was constructed by computer analysis of the data generated from the median effect analysis. CI values <1 occurred over a wide range of inhibition levels, indicating synergy.

diately after the completion of treatment (at day 15) and at day 22 are summarized in Fig.4*d*. More severe body weight loss was observed, ~20% at day 15, in mice treated with 60 mg/kg of gefitinib alone or with CPT-11, suggesting that CPT-11 does not enhance the body weight loss induced by gefitinib. Body weight recovered by day 22 (Fig. 4*e*). No deaths of were observed during the treatment or observation period.

Induction of EGFR phosphorylation and enhanced gefitinib-induced PARP activation by CPT-11

To elucidate the synergistic effects of CPT-11 and gefitinib, we examined the effect of exposure of CPT-11 on EGFR phosphorylation in Lovo and WiDr cells. Phosphorylated EGFR was detected with anti-phosphotyrosine antibody (PY-20)

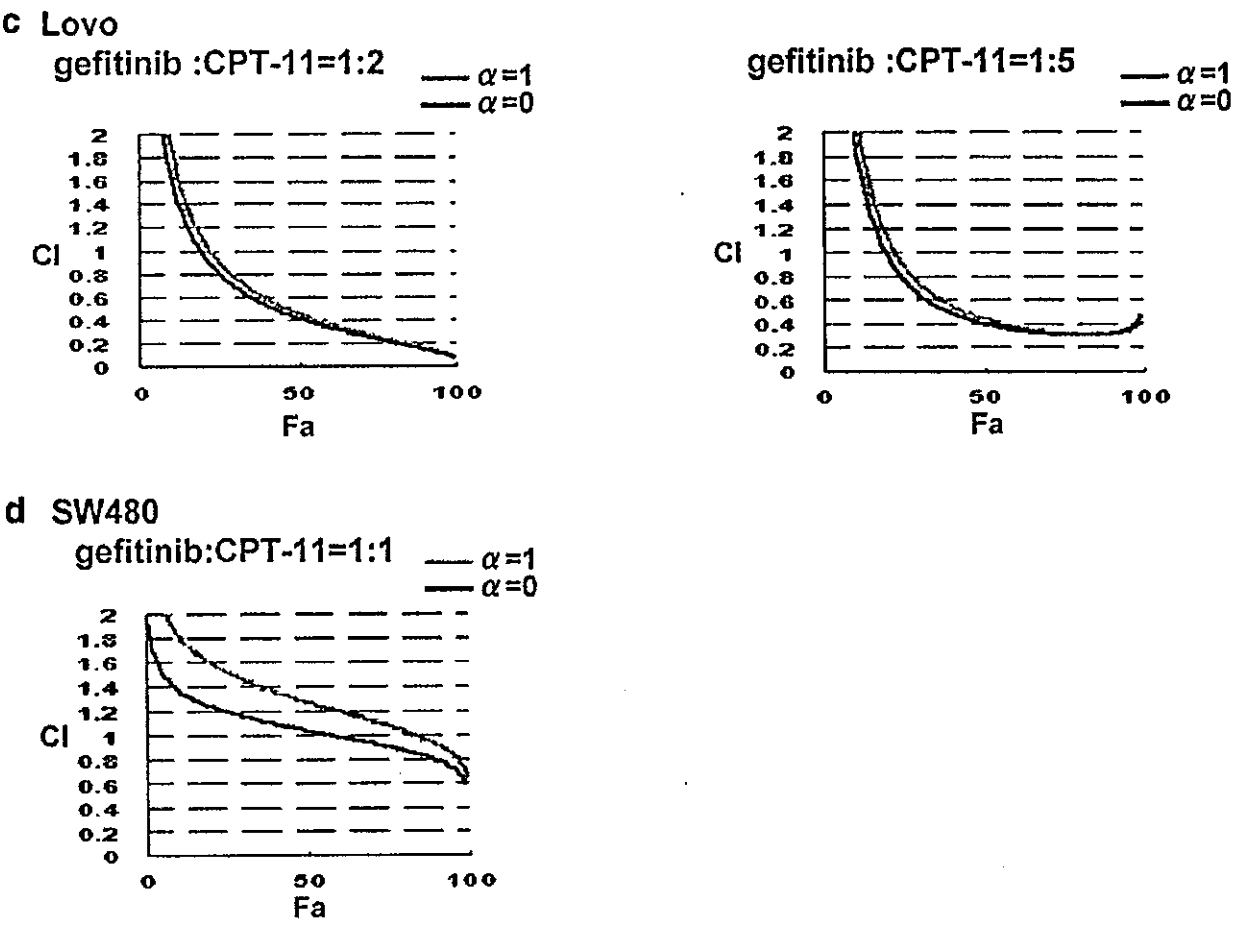

FIGURE 2 – CONTINUED.

against immunoprecipitated EGFR and increased phosphorylation of EGFR was observed after exposure to CPT-11 in Lovo cells in dose- and time- dependent manner (3–24 hr) (Fig. 5*a*). The dose-dependent activation of EGFR by CPT-11 was also obtained in WiDR cells (Fig. 5*b*). CPT-11-induced phosphorylation of EGFR was observed without ligand-stimulation. The EGFR activation was completely inhibited by 24 hd exposure of 5 μM gefitinib. gefitinib-induced apoptosis measured by PARP activation was enhanced by combination with CPT-11, although no PARP activation was induced by CPT-11 alone (Fig. 5*c*). These results suggest that the modification of EGFR by CPT-11 increases the cellular sensitivity to gefitinib, resulting the synergistic effect of CPT-11 and gefitinib. We also observed the effect of gefitinib on the expression and the activity of topoisomerase I by immunoblotting and decatenatnion assay. No modification of topoisomerase I by gefitinib was observed (data not shown).

DISCUSSION

Evidence has suggested that the new EGFR-targeting drug gefitinib is active against gastrointestinal malignancies as well as non-small cell lung cancer. Combination of gefitinib with cytotoxic drugs has been evaluated in the U.S. and Europe,[19,20] but combination with CPT-11 has not been evaluated. CPT-11 is a potent DNA-targeting drug in patients with colorectal cancer that is refractory to treatment with fluorouracil and leucovorin,[4,5] although a higher rate of treatment-induced toxicity was suspected in a retrospective analysis.[7] In preclinical study, Ciadiello *et al.*[17,18] reported that supra-additive combination effect of EGFR-targeting drug (cetuximab or gefitinib) and topoisomerase I inhibitor, topotecan was observed in human colorectal cancer GEO xenograft. We have therefore studied the synergistic potential for a new combination regimen containing CPT-11 and gefitinib. The synergistic potential of CPT-11 combined with gefitinib demonstrated in our study suggests that the gefitinib/CPT-11 combination is a promising regimen for colorectal cancer patients. Schedule 2, administration of oral gefitinib and intravenous CPT-11 designed in a xenograft model, was based on possible clinical administration of the drugs, and thus a treatment schedule consisting of intermittent *i.v.* CPT-11 and continuous gefitinib *p.o.* may be applicable to colorectal cancer in humans.

In xenograft models, body weight loss was observed when administered in combination as well as when each drug was administered alone. However, body weight loss rapidly recovered immediately after the completion of administration, and no deaths were observed. Diarrhea is the dose-limiting toxicity of CPT-11 in humans,[7] and it is also observed in patients treated with gefitinib.[21,22] However, no diarrhea or related phenomena were observed in the mouse model treated with combinations of these

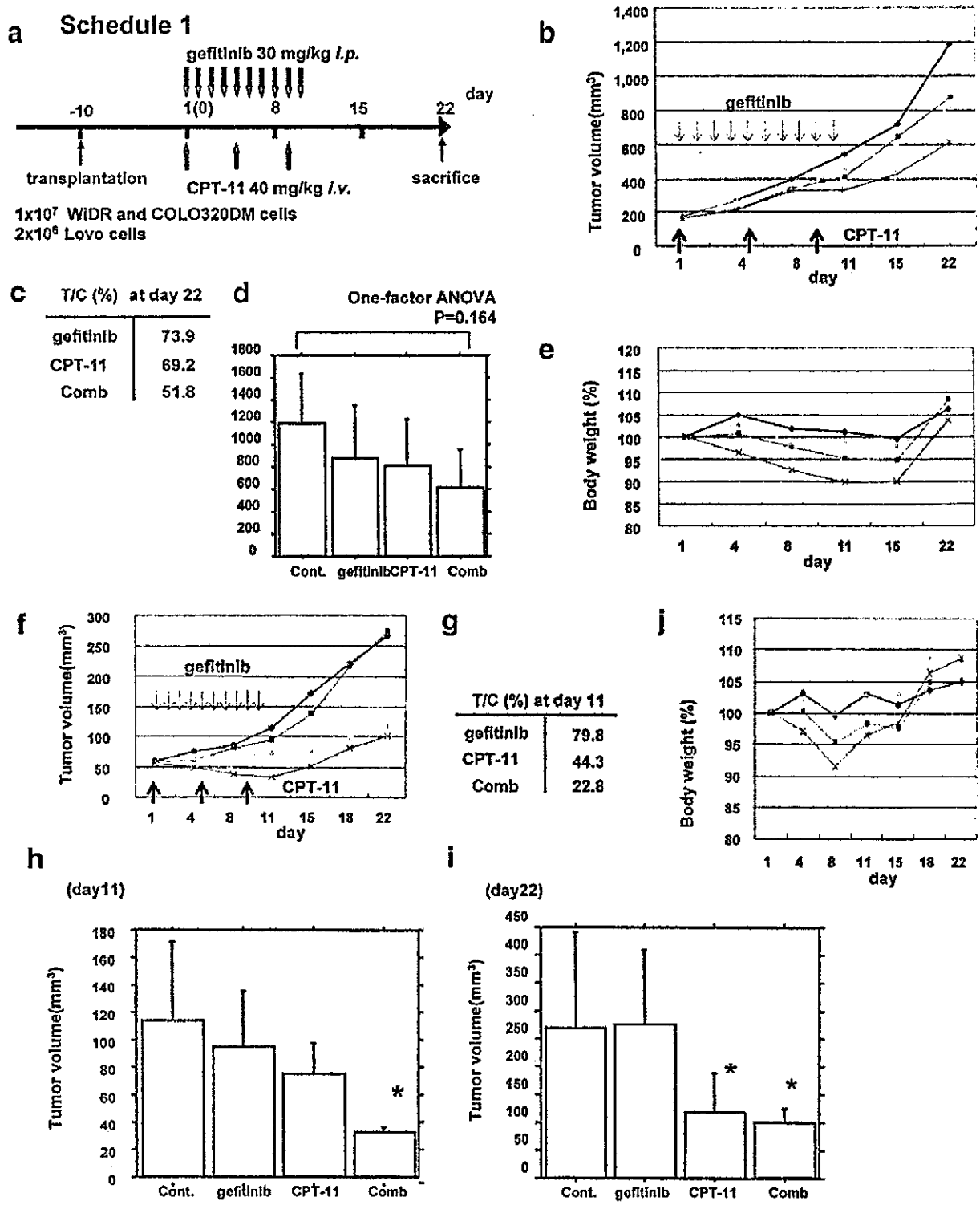

FIGURE 3 – *In vivo* combined effect of gefitinib and CPT-11 on WiDR and Lovo tumor xenografts. (*a*) Treatment schedule. (*b*) (WiDR) and F (Lovo), Tumor growth curves. Female nude mice bearing WiDR or Lovo xenografts were randomly allocated to treatment with 5% (w/v) glucose solution (diamond), gefitinib (square), CPT-11 (triangle), or the combination (×). Tumor volume was calculated as described in Material and Methods. Each data point represents the mean tumor volume of 5 mice. E (WiDR) and J (Lovo) Percent change in body weight in the gefitinib (hatched square) and combination (×) group. C (WiDR) and G (Lovo) Ratio of tumor volume in the control (C) to tumor volume in the treatment group (T) at day 22 and day 15. D (WiDR), H and I (Lovo) Histogram of mean tumor volume at day 11 and day 22 bars, *S.D.* Statistical analysis was performed by 1-factor ANOVA, followed by Fisher's PLSD between 2 groups, as described in the Material and Methods section. *Significant difference ($p<0.05$; Fisher's PLSD) compared to the control.